National Technical University of Athens

School of Civil Engineering

Institute of Structural Analysis & Aseismic Research

MSc Thesis in

"Analysis & Design of Earthquake

Resistant Structures":

Nonlinear Analysis of Frame Structures based on Augmented Total Potential Energy Minimization

by

Charalampos Andriotis

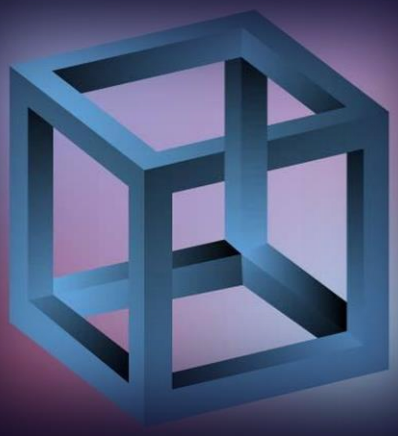

Advisor: Professor Vlasis Koumousis

Athens, 2015

Abstract

MSc Thesis:

Nonlinear Analysis of Frame Structures based on Augmented Total Potential Energy Minimization

by

Charalampos Andriotis

MSc in Analysis and Design of Earthquake Resistant Structures

Institute of Structural Analysis & Aseismic Research

National Technical University of Athens

Advisor: Professor V. K. Koumousis

In this work a new beam – column element for geometrically and material nonlinear analysis of frame structures is presented. The Total Potential Energy functional is augmented by adding new constraint terms with Lagrange multipliers to ensure compatibility and minimization is performed implementing primal – dual nonlinear optimization methods. This procedure generates a hybrid – type finite element, having the rotation θ along the element as the only internal approximated field, derived via a curvature based interpolation. The stress resultants at every position of the element are determined with the cross sections discretized into fibers. The formulation presented fully addresses large displacement theory with no simplifications for curvature and axial deformation. The solution scheme follows the standard Newton – Raphson and arc – length numerical methods to derive the equilibrium path. Validation and verification of the proposed model is performed via comparative analysis with

other beam – column finite elements, solving benchmark nonlinear analysis problems cited in the literature. Numerical results show that the proposed element allows for coarser discretization of the structural members than the standard force based elements, to obtain results of the same accuracy.

Acknowledgments

I wish to express my most sincere gratitude to my advisor, Professor Vlasis Koumousis, for his continued guidance and support during the investigation of the present work. His imaginative spirit and integrated sense in engineering science were a constant source of motivation. His instructions were critical and always helped me to deeper understand the physical and mathematical aspects of structural analysis. Attending the series of his postgraduate lectures on structural optimization, definitely taught me one of the most inspirational perspectives of engineering and this is obviously reflected in this Thesis.

I would also like to thank all the members of Professor's group and especially the PhD candidate Ilias Gkimousis for our creative collaboration during these years. I was happy to discover and discuss with him various aspects of nonlinear finite element analysis and modeling and I am grateful for meeting him.

Financial support for these studies was provided by Onassis Foundation. This financial support encouraged me to complete the MSc program, thus it is gratefully acknowledged.

To the person embracing my "nonlinearities",

my very special,

Ersi.

Table of Contents

Abstract i

Acknowledgments iv

Table of Figures vii

Table of Tables ix

1 Introduction 1

1.1 Nonlinear Structural Analysis 1

1.2 Objectives and Scope 2

2 Nonlinear Optimization: Basic Theory and Methods 4

2.1 Unconstrained Problems 5

2.1.1 Problem determination and Optimality Conditions 5

2.1.2 Steepest Descent Method 6

2.1.3 Newton's Methods 8

2.1.4 Conjugate Direction Methods 9

2.1.5 Illustrative Example 10

2.2 Constrained Problems 11

2.2.1 Problem determination and Optimality Conditions 11

2.2.2 Gradient Projection Method 12

2.2.3 Penalty Methods 14

2.2.4 Barrier Methods 15

2.2.5 Primal – Dual Methods 17

3 Large Displacements and Beam-Column Elements 19

3.1 Kinematics 19

3.2 Variational Principles 21

3.2.1 The TPE functional 22

3.2.2 Generalization of TPE 25

3.3 Fiber Beam – Column Finite Element Formulations 26

4 Primal – Dual Methods for a New Beam-Colum Element 33

4.1 Newton – Raphson Formulation 34

4.1.1 Elemental level 34

4.1.2 Structural level 40

4.2 Arc – Length Formulation 41

5 Examples and Verification 44

5.1 Cantilever beam with vertical load at the tip 44
5.2 Cantilever beam with moment at the tip 46
5.3 Toggle frame 48
5.4 Lee's frame 51
6 Conclusions and Future Research 54
6.1 Concluding Remarks 54
6.2 Future Research 55
References 56

Table of Figures

Figure 1: Steepest Descent Method 6

Figure 2: Newton's Method 8

Figure 3: 3D plot of f(x,y) 10

Figure 4: Steps of different methods 11

Figure 5: Gradient Projection Method 13

Figure 6: Contour and 3D plot of f(x,y) and constraints 16

Figure 7: Contour and 3D view of Barrier methods' modification 16

Figure 8: Kinematic assumptions 20

Figure 9: Strain energy density 23

Figure 10: Fiber beam – column element in local coordinate system 28

Figure 11: Fiber beam – column element in natural system 29

Figure 12: Arc – length method 42

Figure 13: Cantilever under vertical tip load 45

Figure 14: Equilibrium paths for different elastic analyses (free edge) 45

Figure 15: Equilibrium paths for different inelastic analyses (free edge) 46

Figure 16: Deformed shape and comparison between GNEA and GMNIA 46

Figure 17: Cantilever with tip moment 47

Figure 18: Equilibrium paths for different elastic analyses (free edge) 47

Figure 19: Deformed shape and results of GNEA 48

Figure 20: Toggle Frame 49

Figure 21: Equilibrium paths for different elastic analyses (top node) 49

Figure 22: Equilibrium paths for different inelastic analyses (top node) 50

Figure 23: Deformed shape and comparison between GNEA and GMNIA 50

Figure 24: Lee's Frame 51

Figure 25: Equilibrium paths for different elastic analyses (node #) 51

Figure 26: Equilibrium paths for different inelastic analyses (node #) 52

Figure 27: Deformed shape and comparison between GNEA and GMNIA 52

Table of Tables

Table 1: Energy Functionals 21

Table 2: Cantilever Properties 45

Table 3: Cantilever Properties 47

Table 4: Toggle Properties 49

Table 5: Lee's Frame Properties 51

1 Introduction

This work addresses the nonlinear structural analysis of frames. Both geometrical and material nonlinearities are taken into consideration to investigate different features related to nonlinear behavior. Furthermore no simplifications regarding the geometrical nonlinearity are imposed, such as moderate rotations etc. and full kinematic expressions are incorporated. Elastic and inelastic analysis is based on fiber beam – column finite elements, which are suitable and adequate for modeling the behavior of skeletal structures.

1.1 Nonlinear Structural Analysis

Nonlinear phenomena play a significant role and are of great importance in structural analysis. Inelastic behavior is the main material nonlinearity, whereas geometrical nonlinearities turn out to be critical in flexible steel structures. The response of structures accounting for the nonlinear effects may be quite different from the predictions of linear elastic analysis. However, nonlinear considerations require increased computational cost, as they employ iterative methods. Another computational problem is that proper approximations have to be established within the process to derive an accurate solution. In recent years, various researchers dealing with nonlinear structural analysis have focused on developing models capable to overcome these difficulties.

Geometrical nonlinearities should be considered when a flexible structure is subjected to intensive load levels causing large displacements and equilibrium cannot be accurately accounted for in the undeformed and should be enforced at the deformed state. The deformed configuration of the structure is engaged into the path that establishes equilibrium between external and internal forces, as the new geometry differs considerably from the initial one. Material nonlinearity mainly regards the elastoplastic behavior of structures. Plasticity is a key – word for this source of nonlinearity. Hence, material nonlinearities imply that a

structure instead of just storing, also dissipates energy when a yield limit of its members is exceeded demonstrating a hysteretic behavior. As a consequence, irreversible plastic deformations are developed which remain also after the external action is removed.

Various finite elements have been developed for geometrical and material nonlinear analysis of structures. Most of them are based on displacement methods, which imply that strains are related to displacements via polynomial interpolation – shape functions. Due to this interpolation strategy, structural members modeled with displacement based elements require a fine discretization in order to capture the actual response, as they violate equilibrium. The great number of members and consequently degrees of freedom increase computational cost, thus current research work is not in favor of such elements. Hence, force based formulations for deriving structural elements needing coarser discretization are gaining ground. Force based elements are based on the interpolation of the forces along the element, so they satisfy equilibrium but on the other hand they tend to violate compatibility. This fact introduces further nested iterative cycles in the standard solution algorithms in order reach a compatible state. Overall, force based approaches though, have significantly lower computational cost than displacement based methods.

1.2 Objectives and Scope

The objective of this work is to examine the implementation of nonlinear programming into nonlinear analysis of structures. This implementation results in deriving a hybrid – type beam – column finite element on the basis of a generalized Total Potential Energy minimization. Along these lines Saje (1990) has addressed the main features of a similar generalization, following though the assumptions of hyperelasticity. The present element is oriented in incorporating all geometrically nonlinear features, whereas its cross sections are discretized into fibers in order to account for the plastic behavior. Additionally a computer program called NAFS (Nonlinear Analysis of Frame Structures) was developed in Matlab. All analyses regarding the proposed formulation were performed with NAFS.

The remaining parts of this work are organized as follows:

In Chapter 2 the basic theory, methods and algorithms developed within the context of nonlinear optimization are presented. The chapter is subdivided into a section dealing with unconstrained problems and a second one dealing with constrained problems. In the first, methods such as steepest descent methods, Newton's methods and conjugate direction methods are presented, followed by a relevant example. Then for constrained problems primal, penalty, barrier and primal – dual methods are discussed, also including an example for Barrier methods.

Chapter 3 deals with geometrical nonlinearities from theoretical and computational point of view. First, the kinematic relations of the theory of large displacements are presented. Subsequently, the variational principles related to structural analysis are discussed, in order to reveal the concept underlying the different finite element formulations. In the third section the special features that emerge with the existing displacement and force based formulations are briefly presented.

In Chapter 4 a synthesis of the ideas presented in the previous chapter is presented. Primal – dual optimization approach combining the Total Potential Energy and Lagrange multipliers for compatibility is presented. The new element resulting from this procedure is incorporated in both Newton – Raphson and arc – length integrators in order to establish the solution.

In Chapter 5 examples from the literature are presented. They are used to verify and validate the proposed element. For this purpose analyses and comparisons via OpenSees and SeismoStruct are presented. Four examples are presented; a cantilever beam with a vertical load at the free edge, a cantilever beam with a bending moment at the free edge, a toggle frame and the so – called Lee's frame. All these structures reveal interesting physical and numerical characteristics which are discussed in detail.

Finally, in Chapter 6 a summary and conclusions deduced from all parts of the present work are presented, followed with suggestions for future work.

2 Nonlinear Optimization: Basic Theory and Methods

In almost every well-defined problem described by a mathematical description one can allow a number parameters to vary within certain limits and seek the optimal solution minimizing or maximizing a preset objective function subject to a set of constraints. This is of great importance not only in economics but also in physical problems, which are guided from minimal energy principles. In this respect different continuous and discrete linear and nonlinear optimization methods have been developed. Only a small part of these methods are based on a solid mathematical foundation, as for example the linear mathematical programming problems, whereas most of the nonlinear programming and discrete problems are characterized by an enormous complexity allowing for ad-hoc and heuristic methods.

Simplex Method is one of the most popular and reliable methods for the linear programming problem, attaining the optimal solution in a finite number of steps. Moreover, the efficiency of Simplex, shows the way also for nonlinear problems which can be treated approximately as linear ones. For highly nonlinear problems though, realistic linearization adds complexity and increases computational cost. Therefore, development of nonlinear optimization methods is essential.

Nonlinear minimization/maximization problems can be subdivided into two main categories; unconstrained and constrained ones. There have been various methods developed associated with each category. In fact, this categorization is not too strict, as constrained problems can be transformed into unconstrained ones with proper modifications (penalty functions, barrier functions, Lagrange multipliers), thus be solved with the same numerical schemes. In the following sections some of these methods are presented and discussed.

2.1 Unconstrained Problems

2.1.1 Problem determination and Optimality Conditions

The optimization problem can be set in the form,

$$\begin{aligned} &minimize\ f(\boldsymbol{x}) \\ &subject\ to\ \boldsymbol{x}\ \in \Omega \end{aligned} \tag{1}$$

where f is a real – valued function, $\boldsymbol{x}$ a vector of n unknown variables and Ω a subset of E^n. In fact $\boldsymbol{x}$ is restricted in Ω, however this constraint is not of functional form, so that the problem is conventionally considered to belong to the unconstrained family. Completely unconstrained problems demand $\Omega = E^n$. In any case, if f is continuous, defined on the compact set Ω, then f has a minimum point in Ω according to the theorem of Weierstrass.

Also, if $\boldsymbol{x}^*$ is a relative minimum of f, then for any $\boldsymbol{d} \in \Omega$ which is a feasible direction at $\boldsymbol{x}^*$ we have $\nabla f(\boldsymbol{x}^*) \cdot \boldsymbol{d} \geq 0$. In the case of completely unconstrained problems $\boldsymbol{x}^*$ is an interior point of Ω, thus the previous condition reduces to $\nabla f(\boldsymbol{x}^*) = 0$, as $\nabla f(\boldsymbol{x}^*) \cdot \boldsymbol{d} \geq 0$ is forced to stand for any $\boldsymbol{d}$. These two relations are found in the literature as the *first – order necessary conditions*.

Additional conditions can be obtained if we exploit the information given by the Hessian matrix $\nabla^2 f = \left[\frac{\partial^2 f}{\partial x_i \partial x_j}\right]$ and thus they are mentioned as the *second – order necessary conditions*. If $\Omega \subset E^n$ they are expressed in terms of the perpendicular feasible direction to $\nabla f(\boldsymbol{x}^*)$, namely for $\nabla f(\boldsymbol{x}^*) \cdot \boldsymbol{d} = 0$, as $\boldsymbol{d}^T \nabla^2 f(\boldsymbol{x}^*) \boldsymbol{d} \geq 0$. If $\boldsymbol{x}^*$ is an interior point of Ω (that yields $\Omega = E^n$), then $\boldsymbol{d}^T \nabla^2 f(\boldsymbol{x}^*) \boldsymbol{d} \geq 0$ stands for any $\boldsymbol{d}$, without restrictions. This last condition is equivalent to the one stating that the matrix $\nabla^2 f(\boldsymbol{x}^*)$ is positive semidefinite. Alternatively, we can claim that in the case of unconstrained minimization problems, if $\nabla^2 f(\boldsymbol{x}^*)$ is not positive semidefinite, $\boldsymbol{x}^*$ cannot be a minimization vector. When $\nabla^2 f(\boldsymbol{x})$ is symmetric, then $\nabla^2 f(\boldsymbol{x}^*)$ is positive semidifinite if and only if all of its eigenvalues are nonnegative.

Necessary conditions are very important as they explore the properties of the function f in the neighborhood of the solution $\boldsymbol{x}^*$, thus providing a good estimator for the detection of relative optima. However they do not guarantee the existence of minimum at any $\boldsymbol{x}$. Therefore determination of *sufficient conditions* for a relative minimum is significant. In this sense, for unconstrained problems it can be proved that if $\nabla f(\boldsymbol{x}^*) = 0$ and $\nabla^2 f(\boldsymbol{x}^*)$ is positive definite, then $\boldsymbol{x}^*$ is a strict relative minimum point.

In the following sections the above feature will provide a solid ground for the introduction and implementation of some numerical methods which iteratively lead to the optimal solution.

2.1.2 Steepest Descent Method

The method of steepest descent or gradient method is of fundamental importance for the minimization problem and lies on a clear geometric interpretation. Starting from an initial guess of the optimum $\boldsymbol{x}_o$, the normal vector $\boldsymbol{n}_o = \nabla f(\boldsymbol{x}_o)$ of f is determined. Then we search for the minimum value of function f over the hyperplane defined by the gradient. As soon as the minimum is reached the first iteration is completed and the iterative procedure goes on. These steps are illustrated in Figure 1. The algorithm described, can be expressed in terms of the following sequence:

$$\boldsymbol{x}_{k+1} = \boldsymbol{x}_k - a_k \boldsymbol{n}_k \tag{2}$$

where $\boldsymbol{n}_k = \nabla f(\boldsymbol{x}_k)$ and a_k is a positive scalar minimizing $f(\boldsymbol{x}_k - a_k \boldsymbol{n}_k)$

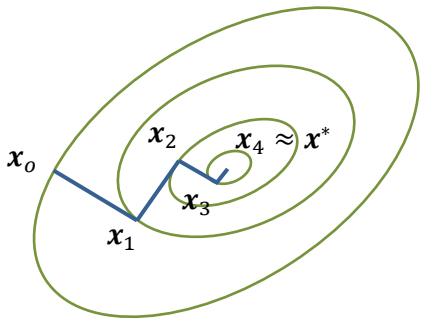

Figure 1: Steepest Descent Method

In the pure quadratic minimization problem calculation of a_k can be obtained explicitly. In this case the function can be defined as:

$$f(\boldsymbol{x}) = \frac{1}{2}\boldsymbol{x}^T\boldsymbol{Q}\boldsymbol{x} - \boldsymbol{b}^T\boldsymbol{x} \quad \textbf{(3)}$$

where $\boldsymbol{Q}$ is a positive definite *nxn* matrix. According to the sufficient conditions presented in the previous section, we can determine the minimum by setting the gradient of f equal to zero:

$$\boldsymbol{Q}\boldsymbol{x}^* - \boldsymbol{b} = \boldsymbol{0} \quad \textbf{(4)}$$

This is a linear equation and thus the minimization point $\boldsymbol{x}^*$ can be determined following the algorithm of steepest descent. However this implies that the matrix $\boldsymbol{Q}$ should be inverted. The steepest descent method avoids this inversion, as it searches for the next point over the hyperplane of the gradient of f. Thus in every step a single – variable function minimization problem emerges with respect to a_k :

$$minimize\ f(\boldsymbol{x}_k - a_k\boldsymbol{n}_k) = \frac{1}{2}(\boldsymbol{x}_k - a_k\boldsymbol{n}_k)^T\boldsymbol{Q}(\boldsymbol{x}_k - a_k\boldsymbol{n}_k) - \boldsymbol{b}^T(\boldsymbol{x}_k - a_k\boldsymbol{n}_k) \quad \textbf{(5)}$$

The above problem has one unique solution derived by the following relation:

$$a_k = \frac{\boldsymbol{n}_k{}^T\boldsymbol{n}_k}{\boldsymbol{n}_k{}^T\boldsymbol{Q}\boldsymbol{n}_k} \quad \textbf{(6)}$$

Hence substituting relation **(6)** into **(5)** we obtain:

$$\boldsymbol{x}_{k+1} = \boldsymbol{x}_k - \left(\frac{\boldsymbol{n}_k{}^T\boldsymbol{n}_k}{\boldsymbol{n}_k{}^T\boldsymbol{Q}\boldsymbol{n}_k}\right)\boldsymbol{n}_k \quad \textbf{(7)}$$

Relation **(7)** offers an explicit formula for determination of every next vector of the sequence of the steepest decent method in the quadratic case.

2.1.3 Newton's Methods

Consider that function f satisfies the second – order sufficient condition at $\boldsymbol{x}^*$, namely the Hessian matrix $\nabla^2 f(\boldsymbol{x}^*)$ is positive definite. Then the minimization problem reduces to the solution of the zero stationary value condition:

$$\nabla f(\boldsymbol{x}^*) = \boldsymbol{0} \tag{8}$$

which is in fact an algebraic relation. Thus, a Newton type numerical scheme can be implemented, in order to determine the optimum point $\boldsymbol{x}^*$:

$$\boldsymbol{x}_{k+1} = \boldsymbol{x}_k - a_k[\nabla^2 \boldsymbol{f}_k]^{-1}\boldsymbol{n}_k \tag{9}$$

where $\nabla^2 \boldsymbol{f}_k = \nabla^2 f(\boldsymbol{x}_k)$ and a_k is a positive scalar minimizing $f(\boldsymbol{x}_k - a_k[\nabla^2 \boldsymbol{f}_k]^{-1}\boldsymbol{n}_k)$. In case that $a_k = 1$ the standard Newton – Raphson formula is obtained. However, if the initial point of sequence **(9)** $\boldsymbol{x}_o$ is not sufficiently close to the solution, significance of nonquadratic terms is enhanced and objective function might increase. Introduction of parameter a_k prevents this undesirable possibility. This case leads to a modified Newton method.

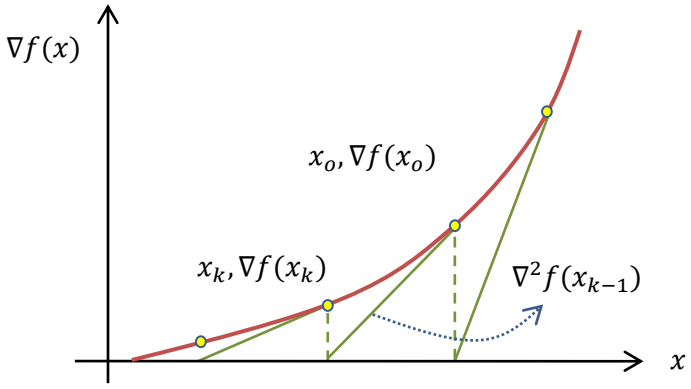

Figure 2: Newton's Method

In problems with a great number of variables, where inversion of the Hessian matrix in every iteration is computationally inefficient, it can be kept constant throughout the iterations. This concept results an increase number of iterations, but might decrease time. Relation **(9)** is modified as:

$$\boldsymbol{x}_{k+1} = \boldsymbol{x}_k - a_k[\nabla^2 \boldsymbol{f}_o]^{-1}\boldsymbol{n}_k \tag{10}$$

2.1.4 Conjugate Direction Methods

In this section Conjugate Direction methods are briefly presented. These methods are between the method of Steepest Descent and the Newton's method. First they are employed for the analysis of the quadratic programming problem and subsequently the resulting scheme is extended to the nonquadratic case. The *Conjugate Direction Theorem* for the quadratic problem **(3)**, where $\boldsymbol{Q}$ is a nxn matrix, gives that the sequence:

$$\boldsymbol{x}_{k+1} = \boldsymbol{x}_k - a_k \boldsymbol{d}_k \tag{11}$$

$$a_k = \frac{\boldsymbol{n}_k{}^T \boldsymbol{d}_k}{\boldsymbol{d}_k{}^T \boldsymbol{Q} \boldsymbol{d}_k} \tag{12}$$

where $\{\boldsymbol{d}_i\}_{i=0}^{n-1}$ is a set of Q – orthogonal nonzero vectors, converges to the minimum $\boldsymbol{x}^*$ after n iterations. This theorem is in fact an orthogonal expansion for the solution of equation **(9)**.

One of the Conjugate Directions Methods, is the so – called Conjugate Gradient Method. This method taking first a pure steepest descent step, afterwards adapts the direction of search according to a conjugate direction coming from linear combination of the new and the old gradient. Its attractiveness is based on its simple straightforward explicit formula:

$$\begin{aligned} \boldsymbol{x}_{k+1} &= \boldsymbol{x}_k - a_k \boldsymbol{d}_k \\ a_k &= \frac{\boldsymbol{n}_k{}^T \boldsymbol{d}_k}{\boldsymbol{d}_k{}^T \boldsymbol{Q} \boldsymbol{d}_k} \\ \boldsymbol{d}_{k+1} &= \beta_k \boldsymbol{d}_k + \boldsymbol{n}_{k+1} \\ \beta_{k+1} &= \frac{\boldsymbol{n}_{k+1}{}^T \boldsymbol{d}_k}{\boldsymbol{d}_k{}^T \boldsymbol{Q} \boldsymbol{d}_k} \end{aligned} \tag{13}$$

with initial value $\boldsymbol{d}_o = \boldsymbol{n}_o$. It can be proved that the Conjugate Gradient Method presented above is a Conjugate Direction Method.

The technique of Conjugate Gradient Method can be extended to nonquadratic problems. What we have to modify in comparison with the quadratic problem formulation is to replace

matrix $\boldsymbol{Q}$ with $\nabla^2 \boldsymbol{f}_k$. In fact this modification implies the assumption that the initial guess $\boldsymbol{x}_o$ is sufficiently close to $\boldsymbol{x}^*$, so that f is well approximated by a quadratic one. In this sense it is possible that more than n steps might be needed for convergence. After n steps we can either continue on the new conjugate directions produced by the algorithm, or interrupt and start again replacing $\boldsymbol{x}_o = \boldsymbol{x}_n$.

2.1.5 Illustrative Example

Let us consider the following two - variable quadratic function for the unconstrained minimization problem:

$$f(x,y) = 5x^2 + 5xy + 15y^2 - 10x - y$$

Function f can be depicted in a 3D space as shown in **Figure 3**. The minimum point appears at:

$$\begin{Bmatrix} x^* \\ y^* \end{Bmatrix} = \begin{Bmatrix} +1.074 \\ -0.146 \end{Bmatrix}$$

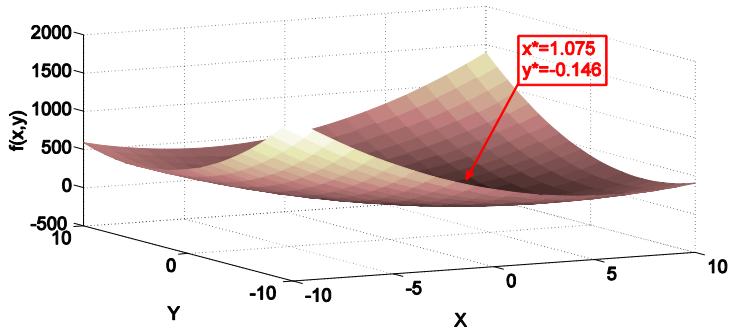

Figure 3: 3D plot of f(x,y)

For the solution of this minimization problem the above three methods where employed; Steepest Descent Method (SDM), Newton's Method (NM) and Conjugate Gradient Method (CGM). In **Figure 4** their convergence paths are depicted.

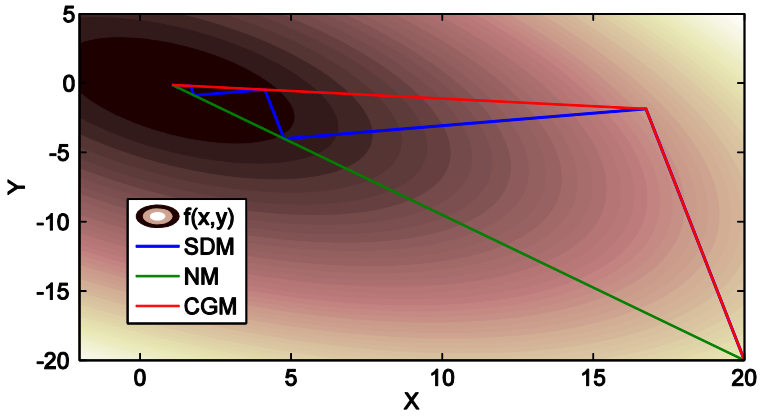

Figure 4: Steps of different methods

Notice that the Steepest Descent Method has a slower convergence due to the zig – zag path produced. On the other hand Newton's Method converges in one iteration, because the quadratic features of function f are eliminated due to the Hessian information that the method implies. The Conjugate Gradient Method, as mentioned before, reveals an intermediate convergence behavior, starting from an initial step which coincides with the Steepest Descent Method steps.

2.2 Constrained Problems

2.2.1 Problem determination and Optimality Conditions

The general constrained optimization problem is set as:

$$\begin{aligned} &minimize \quad f(\boldsymbol{x}) \\ &subject\ to \quad \boldsymbol{h}(\boldsymbol{x}) = \boldsymbol{0} \\ &\qquad\qquad \boldsymbol{g}(\boldsymbol{x}) \leq \boldsymbol{0} \\ &\qquad\qquad \boldsymbol{x} \in \Omega \subseteq E^n \end{aligned} \qquad \textbf{(14)}$$

where $(\boldsymbol{x}) = \{h_1 \quad h_2 \quad \dots \quad h_m\}$,$\boldsymbol{g}(\boldsymbol{x}) = \{g_1 \quad g_2 \quad \cdots \quad g_p\}$, are two sets of equality and inequality constraints respectively.

It is important again to establish the necessary conditions at a local optimum point $\boldsymbol{x}^*$. The *first – order necessary optimality conditions*, in the case of the generalized minimization

problem, are also known as the Karush – Kuhn – Tucker Condition. They state that if $\boldsymbol{x}^*$a relative minimum, feasible and regular point for all the constraints, then:

$$\nabla f(\boldsymbol{x}^*) + \nabla \boldsymbol{h}^T(\boldsymbol{x}^*) \cdot \boldsymbol{\lambda} + \nabla \boldsymbol{g}^T(\boldsymbol{x}^*) \cdot \boldsymbol{\mu} = 0$$
$$\{\mu_i \cdot g_i(\boldsymbol{x}^*)\}_{i=1}^{p} = \mathbf{0} \qquad \textbf{(15)}$$
$$\boldsymbol{\mu} \geq \mathbf{0}$$

where $\boldsymbol{\lambda} \in E^m$, $\boldsymbol{\mu} \in E^p$. The second of relations **(15)** represent the *complementary slackness* condition, which implies that when $\mu_i > 0$, then $g_i(\boldsymbol{x}^*) = 0$ and when $\mu_i = 0$, then $g_i(\boldsymbol{x}^*) < 0$. In accordance with stationary equation, it is helpful to introduce the *Lagrangian*,

$$L(\boldsymbol{x}, \boldsymbol{\lambda}, \boldsymbol{\mu}) = f(\boldsymbol{x}) + \boldsymbol{h}(\boldsymbol{x}) \cdot \boldsymbol{\lambda} + \boldsymbol{g}(\boldsymbol{x}) \cdot \boldsymbol{\mu} \qquad \textbf{(16)}$$

The *second – order optimality conditions*, as discussed in paragraph 2.1.1, exploit the information of the Hessian matrices. Thus, if $\boldsymbol{x}^*$ is a relative minimum, feasible and regular point then there is a $\boldsymbol{\lambda} \in E^m$ and a $\boldsymbol{\mu} \geq \mathbf{0} \in E^p$, such that:

$$\nabla^2_{xx} L(\boldsymbol{x}^*, \boldsymbol{\mu}, \boldsymbol{\lambda}) = \nabla^2 f(\boldsymbol{x}^*) + \nabla^2 h(\boldsymbol{x}^*) \cdot \boldsymbol{\lambda} + \nabla^2 g(\boldsymbol{x}^*) \cdot \boldsymbol{\mu} \qquad \textbf{(17)}$$

is positive semidefinite in the tangent subspace of the active constraints. These are the *second – order necessary optimality conditions*. If the Hessian $\nabla^2_x L$ is positive definite in the tangent subspace of the active constraints, here come the *second – order sufficient optimality conditions*, thus Karush – Kuhn – Tucker relations result a strict relative minimum at $\boldsymbol{x}^*$.

2.2.2 Gradient Projection Method

The Gradient Projection Method is a primal method, namely solves the nonlinear constrained problem without using dual information. In fact it is based on the *active set strategy* using only the dual information resulting from the active constraints. Active set algorithms, start from a feasible point lying on a predefined guess for the active set of constraints. If there

exists a constraint g_i such that $\mu_i < 0$, the respective constraint is rejected from the active set, as relaxation of g_i will decrease the objective function. On the other hand, if during the progress of the iteration a new constraint appears, it is added in the active set. These choices allow for removing or adding constraints throughout the iterative algorithmic procedure, until the Karush – Kuhn – Tucker conditions are satisfied in the tangent subspace of the active set of constraints.

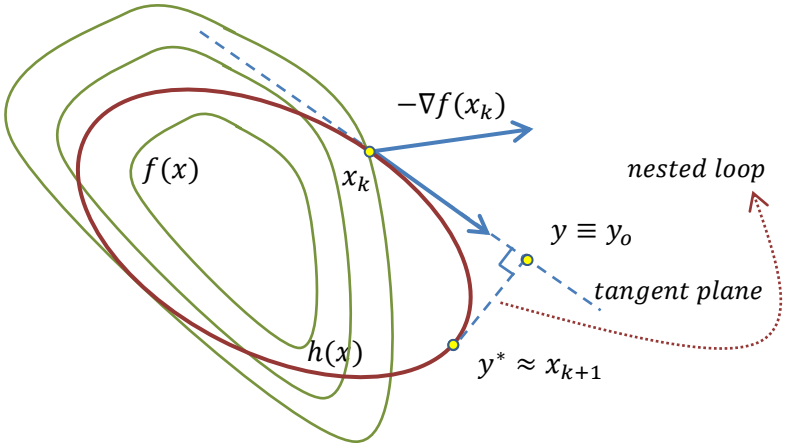

Figure 5: Gradient Projection Method

Consider now the problem **(14)**. The basic idea of Gradient Projection Mehod, is that having determined the working active set and starting from a feasible point $\boldsymbol{x}_k$, we project the negative gradient of f on the tangent plane. That defines the direction of a next point $\boldsymbol{y}$ and a move is made in the direction perpendicular to the tangent plane of the active set, defining an iterative procedure until the constraint surface reaches point y^*.

Representing the active set of constraints as $\boldsymbol{h}(\boldsymbol{x}) = 0$, the projection matrix at $\boldsymbol{x}_k$ is written:

$$P_k = I - \nabla h^T(x_k)[\nabla h(x_k) \cdot \nabla h^T(x_k)]^{-1} \nabla h(x_k) \qquad \textbf{(18)}$$

Once the point $\boldsymbol{y}$ is found on the direction $-P_k \cdot \nabla f(x_k)$, we search for a point y^* of a form

$$y^* = y_o + \nabla h^T(x_k) \cdot a \qquad \textbf{(19)}$$

such that $h(y^*) = 0$, which implies a solution of a nonlinear equation with respect to a. Thus, introducing a Newton – Raphson numerical scheme we finally obtain:

$$y_{j+1} = y_j - \nabla h^T(x_k)\left[\nabla h(y_j) \cdot \nabla h^T(x_k)\right]^{-1} h(y_j) \quad \textbf{(20)}$$

The sequence derived in **(20)** converges to $y^* = x_{k+1}$ and the respective iterations are repeated in every major loop (index k). The entire procedure described above is geometrically depickted in Figure 5.

2.2.3 Penalty Methods

Penalty Methods offer an unconstrained approximation of a constraint optimization problem. Within this idea, for a minimization problem, the objective function is enhanced with some penalty terms, which add a high cost if constraints violated. For a problem of n variables and m equality and p inequality constraint Penalty Methods act directly in an n – dimensional space. Thus, the constraints are in fact eliminated, as they are incorporated smoothly in the objective function. Once the transition to the unconstrained problem has been formulated, the numerical schemes of section 2.1 can be implemented. In a standard problem with only equality constraints of the form:

$$\begin{aligned} &minimize \quad f(\boldsymbol{x}) \\ &subject\ to \quad \boldsymbol{h}(\boldsymbol{x}) = \mathbf{0} \end{aligned} \quad \textbf{(21)}$$

introducing the penalty terms the problem is cast in an unconstrained form as:

$$minimize\ f(x) + \frac{1}{2} c\ |h(x)|^2 \ \ or \ \ f(x) + \frac{1}{2}\ \frac{|h(x)|^2}{tol^2} \quad \textbf{(22)}$$

for some large constant c or some small tol. Quantity $tol = 1/\sqrt{c}$ plays the role of a tolerance value, while power of $|h(x)|$ (can be larger than quadratic) accounts for the sensitivity in tolerance exceedance. From a theoretical point of view c is in fact a parameter leading to a sequence of problems such that $c_k \to \infty$, which implies a additional

computational cost where starting form a c_o the minimization problem is solved until convergence in a number of steps.

2.2.4 Barrier Methods

Barrier Methods, also known as *Interior Point Methods*, are quite analogous to the penalty methods. They also reduce the optimization problem to an n –dimensional variable space. The difference is that in this case the barrier function $B(x)$ tends to infinity as x hits the constraints, while $\mu = \mu_k \to 0$. Thus the auxiliary function takes the following form:

$$\begin{gathered} for\ each\ k \\ minimize\ f(x) + \mu_k \cdot B(x) \end{gathered} \tag{23}$$

Considering the problem **(14)** with only inequality constraints, we can introduce the following barrier function:

$$B(x) = \sum_{i=1}^{p} \frac{-1}{g_i(x)} \tag{24}$$

In addition, it is proved that the logarithmic barrier function, known as *Frisch's logarithmic barrier function*, also admits convergence:

$$B(x) = -\sum_{i=1}^{p} \ln(-g_i(x)) \tag{25}$$

Thus, once the auxiliary function is obtained, we can use any of the methods presented for the unconstrained case to solve the problem.

Illustrative Example

This example aims at investigating the difference between the initial objective function f and the auxiliary function q, which incorporates the constraints in the form of barrier functions. For the nonlinear programming problem designated below:

$$\begin{aligned} minimize \quad & f(x,y) = (x-2)^2 + (y-2)^2 \\ subject\ to \quad & x + y \leq 1 \\ & x, y \geq 0 \end{aligned}$$

In **Figure 6** the contour and the surface obtained by the function f are depicted. The contour is defined by concentric cycles, having their center at the point $(2,2)$, while the constraints are depicted by the isosceles triangle $(1,0)(0,0)(0,1)$.

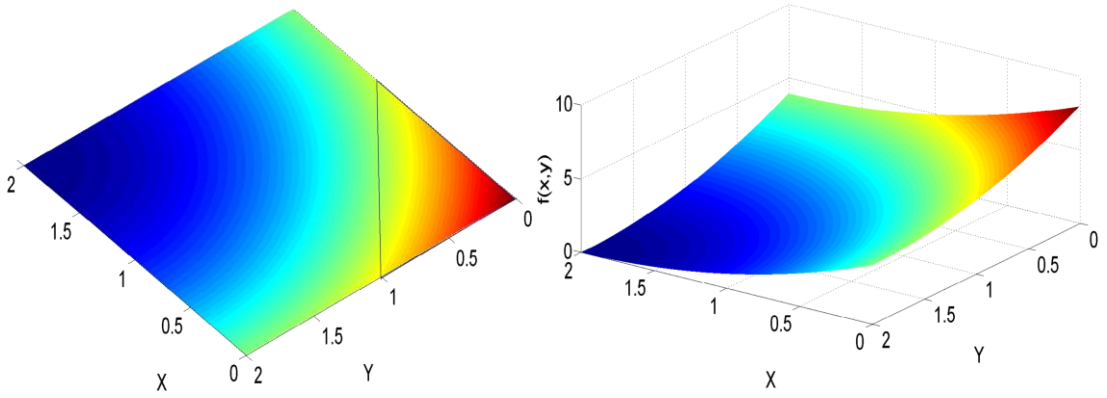

Figure 6: Contour and 3D plot of f(x,y) and constraints

Introducing barrier functions (for a fixed $\mu = \mu_k = 0.3$) accounting for the constraints we can solve the following problem:

$$minimize\ q(x,y) = (x-2)^2 + (y-2)^2 + \mu_k \cdot \left(\frac{1}{x} + \frac{1}{y} + \frac{1}{1-x-y}\right)$$

The shape of function $q(x,y)$ is illustrated in Figure 6. We can notice how the contour is changed near the solution, creating a relative minimum. In the 3D view we can see how the barrier functions affect the initial surface of f, creating a "bowl" which prevents the interior point path from exceeding the bounds and traps the point near the solution.

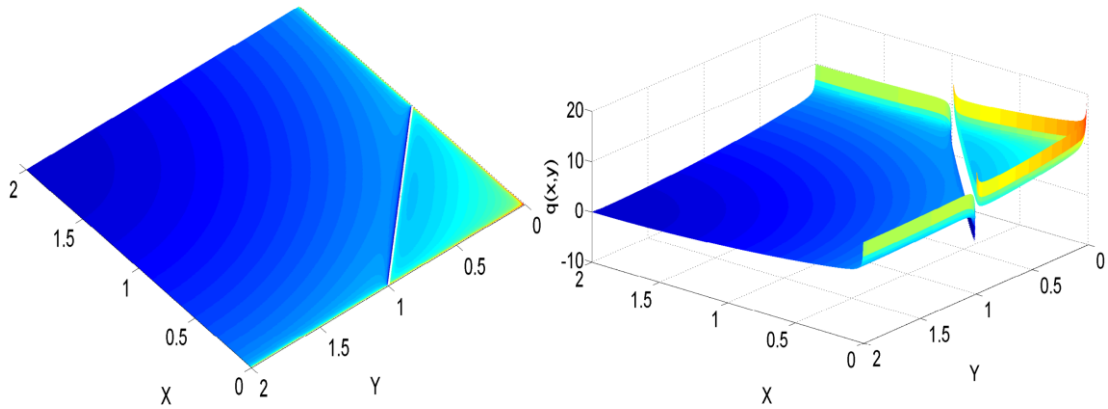

Figure 7: Contour and 3D view of Barrier methods' modification

2.2.5 Primal – Dual Methods

In section 2.2.1 we introduced Lagrange multipliers in order to establish the Karush – Kuhn – Tucker optimality conditions. In fact Lagrange multipliers are the solution of the dual problem. Thus the methods evaluating both primal variables and Lagrange multipliers are termed Primal – Dual Methods. These methods constitute an additional form to convert a primal constrained problem to a primal – dual unconstraint one. In this case though the space of the variables is $(n+m)$, where m is the number of equality constraints. In the case of problems with only equality constraints with Newton's Method selected for the solution process, which is the case implemented in the present work, the KKT conditions reduce to following one single equation:

$$\begin{matrix} \nabla_x L(x,\lambda) = \nabla f(x) + \nabla \boldsymbol{h}^T(x) \cdot \boldsymbol{\lambda} = \mathbf{0} \\ \nabla_\lambda L(x,\lambda) = h(x) = 0 \end{matrix} \Leftrightarrow \quad \nabla L(x,\lambda) = 0 \tag{26}$$

We also assume that $\nabla^2_{xx} L$ is convex, thus positive definite at the solution x^*, so that relation **(26)** is a sufficient condition of the global minimum. Implementing the Newton's Method we obtain:

$$\nabla^2 L(x_k,\lambda_k) \cdot \Delta y_k + \nabla L(x_k,\lambda_k) = 0 \Leftrightarrow$$

$$\begin{bmatrix} \nabla^2 f(x_k) + \nabla^2 \boldsymbol{h}^T(x_k) \cdot \boldsymbol{\lambda}_k & \nabla \boldsymbol{h}^T(x_k) \\ \nabla \boldsymbol{h}(x_k) & \mathbf{0} \end{bmatrix} \cdot \begin{bmatrix} \Delta x_k \\ \Delta \lambda_k \end{bmatrix} + \begin{bmatrix} \nabla f(x_k) + \nabla \boldsymbol{h}^T(x_k) \cdot \boldsymbol{\lambda}_k \\ h(x_k) \end{bmatrix} = \mathbf{0} \tag{27}$$

It should be noted that equation **(27)** due to its special feature can be expressed as follows:

$$\begin{bmatrix} \nabla^2 f(x_k) + \nabla^2 \boldsymbol{h}^T(x_k) \cdot \boldsymbol{\lambda}_k & \nabla \boldsymbol{h}^T(x_k) \\ \nabla \boldsymbol{h}(x_k) & \mathbf{0} \end{bmatrix} \cdot \begin{bmatrix} \Delta x_k \\ \lambda_{k+1} \end{bmatrix} + \begin{bmatrix} \nabla f(x_k) \\ h(x_k) \end{bmatrix} = \mathbf{0} \tag{28}$$

Once Δx_k is calculated, the next point of the method can be obtained by the updating equation

$$x_{k+1} = x_k + \Delta x_k \tag{29}$$

Equations **(27)** and **(28)** can be solved either inverting the matrix $\nabla^2 L(x_k,\lambda_k)$, also termed as *direct step*, or by introducing a secondary quadratic problem. The last concept defines the big

category of *sequential quadratic programming methods* and is based on the similarities between equation **(27)** and the following problem:

$$\begin{aligned} &minimize \quad \nabla f(x_k) \cdot \Delta x_k + \frac{1}{2} \Delta x_k{}^T \cdot \nabla^2_{xx} L(x_k) \cdot \Delta x_k \\ &subject\ to \quad \nabla \boldsymbol{h}(x_k) \cdot \Delta x_k + h(x_k) = 0 \end{aligned} \qquad \textbf{(30)}$$

The minimum point Δx_k of the above quadratic problem can be obtained implementing any of the methods described in the previous sections. In other words the sequential quadratic methods introduce a pure quadratic subproblem in every Newton step. In practice this may be efficient for some large problems as inversion of $\nabla^2 L(x_k, \lambda_k)$ is avoided.

3 Large Displacements and Beam-Column Elements

3.1 Kinematics

The term *kinematics* is referred to the relation between displacements and strains. In the theory of large displacements three different types of strains have been proposed. The simplest one, which is also quite convenient for the engineering practice, is the *rotated engineering strain*:

$$\varepsilon_o = \frac{ds - dx}{dx} \tag{31}$$

A second one is the *Green's strain* which is quite popular in the nonlinear finite element analysis methods:

$$\varepsilon_o = \frac{ds^2 - dx^2}{2 \cdot dx^2} \tag{32}$$

Finally, the *rotated log – strain* can be defined by the following expression:

$$\varepsilon_o = ln\left(\frac{ds}{dx}\right) \tag{33}$$

where in all cases the infinitesimal lengths ds, dx refer to the current and initial configuration respectively, as depicted in Figure 8. From the geometry in Figure 8 we obtain that

$$ds = \sqrt{(du + dx)^2 + dv^2} \tag{34}$$

Substituting relation **(34)** into **(31)** the kinematic relation of the curved axis is derived:

$$\varepsilon_o = \sqrt{(u_x + 1)^2 + {v_x}^2} - 1 \tag{35}$$

where index x denotes differentiation with respect to x. Considering the first term of the Taylor expansion of expression $\sqrt{(u_x + 1)^2 + {v_x}^2}$ we obtain:

$$\varepsilon_o = u_x + \frac{1}{2}({u_x}^2 + {v_x}^2) \tag{36}$$

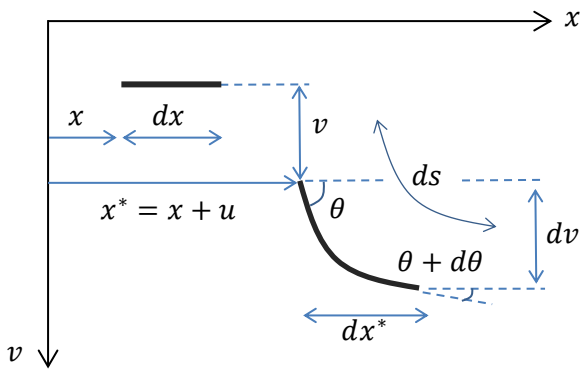

Figure 8: Kinematic assumptions

Notice that relation **(36)** representing the axial deformation can be also obtained by substituting **(35)** into the Green's strain expression **(32)**. Relation **(36)** is of a very convenient form for introducing strains in the finite element methods, as each term is added individually. By the geometric interpretation of the deformed configuration depicted in Figure 8, neglecting $d\theta$, follows that:

$$sin\theta = \frac{dv}{ds}$$
$$cos\theta = \frac{dx^*}{ds} = \frac{du + dx}{ds} \quad \textbf{(37)}$$

Taking into account relation **(31)**, the above expressions result into the following form:

$$sin\theta = \frac{dv}{(\varepsilon_o + 1)dx}$$
$$cos\theta = \frac{du + dx}{(\varepsilon_o + 1)dx} \quad \textbf{(38)}$$

What is additionally needed for the establishment of the Euler – Bernoulli beam theory is the curvature of the cross sections, which is:

$$\kappa = -\frac{d\theta}{ds} = -\frac{d\theta}{(\varepsilon + 1)dx} \quad \textbf{(39)}$$

Note that based on relation **(39)** we can define another curvature κ^* which is a curvature accounting for elongation of the beam axis:

$$\kappa^* = -\frac{d\theta}{dx} = (\varepsilon + 1)\kappa \tag{40}$$

Combining relations **(38)** and differentiating with respect to x we can derive the kinematic expression for the curvature:

$$\frac{d}{dx}(tan\theta) = \frac{d}{dx}\left(\frac{v_x}{u_x + 1}\right) \Longrightarrow$$

$$\kappa = -\frac{(1 + u_x)v_{xx} - u_{xx}v_x}{[(1 + u_x)^2 + {v_x}^2]^{\frac{3}{2}}} \tag{41}$$

$$\kappa^* = -\frac{(1 + u_x)v_{xx} - u_{xx}v_x}{(1 + u_x)^2 + {v_x}^2} \tag{42}$$

In accordance with the Euler – Bernoulli assumptions that plane sections remain plane, we can determine the strain of every fiber from the following relation:

$$\varepsilon = \varepsilon_o - y \cdot \kappa^* \tag{43}$$

where y is the distance from the axis of the beam to every fiber.

3.2 Variational Principles

The Calculus of Variations is a mathematic field dealing with the stationary property of a function of functions, namely a functional. In structural analysis stationary of energy functionals is achieved if and only if the structural system is in equilibrium with external forces. Many functionals have been proposed, its one having different independent-master and dependent – slave fields. Table 1 summarizes all these variations of the energy potentials.

Table 1: Energy Functionals

#	Type	Master Fields	Name
I	Single – field	Displacements	Total Potential Energy (TPE)

II	Single – field	Stresses	Total Complementary Potential Energy (TCPE)
III	Single – field	Strains	-
IV	Two – field	Displacement & Stresses	Hellinger – Reissner (HR)
V	Two – field	Displacement & Strains	-
VI	Two – field	Strains & Stresses	-
VII	Three – field	Displacements, Strains & Stresses	Veubeke – Hu – Washizu (VHW)

3.2.1 The TPE functional

Before presenting the variational problem, it is important to introduce first the strain energy density and complementary strain energy density concepts. These quantities are integrated over the volume of the element examined, expressing the (internal) elastic energy stored. In the uniaxial tension problem strain energy density is defined as:

$$W = \int_0^{\varepsilon} \sigma(\varepsilon')d\varepsilon' \tag{44}$$

while complementary strain energy is:

$$W_c = \int_0^{\sigma} \varepsilon(\sigma')d\sigma' \tag{45}$$

As depicted in Figure 9 it is obvious that we can write the following relation:

$$W + W_c = \sigma \cdot \varepsilon \tag{46}$$

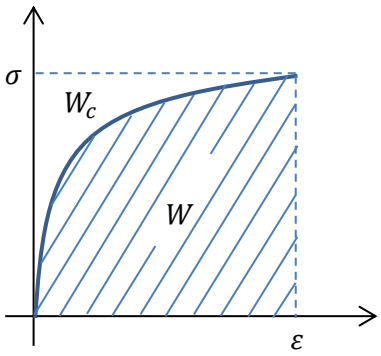

Figure 9: Strain energy density

The Total Potential Energy Functional, also termed the primal functional, considers the displacements as the master field, in other words only displacements are subject to variation. The primal functional can be expressed as follows for the linear elastic problem of a beam – column element:

$$\Pi_{TPE}(u,v) = \frac{1}{2}\iiint_V \sigma^T \varepsilon \, dV - Q^T q \tag{47}$$

Substituting relation **(43)** into **(47)** and assuming that the material satisfies the Hook law with modulus of elasticity E we obtain:

$$\begin{aligned}\Pi_{TPE}(v,u) &= \frac{1}{2}\int_0^l \iint_A \left(E{\varepsilon_o}^2 + Ey^2{\kappa^*}^2 - 2Ey\varepsilon_o\kappa^*\right) dA\, dx - Q^T q \\ &= \frac{1}{2}\int_0^l (EA{\varepsilon_o}^2 + EI{\kappa^*}^2 - 2ES\varepsilon_o\kappa^*)dx - Q^T q\end{aligned} \tag{48}$$

For the case of large displacements but moderate rotations and also symmetric cross section $(S = 0)$, it turns out that $\varepsilon_o = u_x + \frac{1}{2}{v_x}^2$ and $\theta = v_x$, and TPE yields:

$$\Pi_{TPE}(v,u) = \frac{1}{2}\int_0^l \left[EA\left({u_x}^2 + \frac{1}{4}{v_x}^4 + u_x{v_x}^2\right) + EI{v_{xx}}^2\right]dx - Q^T q \qquad \textbf{(49)}$$

Stationary of functional **(49)** implies that the first variation should be zero:

$$\delta\Pi_{TPE}(v,u) = \frac{1}{2}\delta\int_0^l \left[EA\left({u_x}^2 + \frac{1}{4}{v_x}^4 + u_x{v_x}^2\right) + EI{v_{xx}}^2\right]dx - Q^T\delta q = 0 \qquad \textbf{(50)}$$

After some systematic integrations by parts following the calculus of variations the following expression is derived:

$$\begin{aligned}\delta\Pi_{TPE}(u,v) = &-\int_0^l EA(u_{xx} + v_x v_{xx})\delta u\, dx \\ &-\int_0^l EA\left(v_{xx}u_x + v_x u_{xx} + \frac{3}{2}{v_x}^2 v_{xx}\right)\delta v\, dx \\ &+\int_0^l EIw_{xxxx}\delta v\, dx - (Q - Q_{int})^T\delta q = 0\end{aligned} \qquad \textbf{(51)}$$

Equation **(51)** is satisfied for all admissible independent variations of δu,δv,δq, thus all the integrals should be set to zero and the so-called Euler – Lagrange equations can be obtained as:

$$\begin{aligned}EA(u_{xx} + v_x v_{xx}) &= 0 \\ EA\left(v_{xx}u_x + v_x u_{xx} + \frac{3}{2}{v_x}^2 v_{xx}\right) - EIw_{xxxx} &= 0 \\ (Q - Q_{int}) &= 0\end{aligned} \qquad \textbf{(52)}$$

Let us consider the constitutive relations $N = EA(u_{xx} + \frac{1}{2}{v_x}^2)$ and $= EIv_{xx}$. Then the above equations are obtaining the familiar form of the equilibrium equations along with the natural boundary conditions:

$$\frac{dN}{dx} = 0$$

$$Nv_{xx} - \frac{d^2M}{dx^2} = 0 \qquad \textbf{(53)}$$

$$(Q - Q_{int}) = 0$$

3.2.2 Generalization of TPE

The TPE functional can be generalized using Lagrange multipliers. This method yields a family of variational principles including all cases presented in Table 1. The most generic three – field functional, after Veubeke – Hu – Washizu, results from considering the Lagrange multipliers $M(x), N(x)$ for the kinematic restrictions $\varepsilon_o = u_x + \frac{1}{2}{v_x}^2$ and $\kappa = \kappa^* = v_{xx}$, thus **(50)** is expressed as:

$$\Pi_{VHW}(v, u, \varepsilon_o, \kappa, N, M) = \frac{1}{2}\int_0^l (EA{\varepsilon_o}^2 + EI\kappa^2)dx + \int_0^l \left(-\varepsilon_o + u_x + \frac{1}{2}{v_x}^2\right) N\, dx$$

$$\int_0^l (-\kappa + v_{xx})M\, dx - Q^T q \qquad \textbf{(54)}$$

After some calculations, the first variation of the VHW functional results:

$$\delta\Pi_{VHW} = \int_0^l (M + EI\kappa)\delta\kappa + \left(\frac{d(Nv_x)}{dx} - M_{xx}\right)\delta v + (-\kappa + v_{xx})\delta M\, dx$$

$$\int_0^l (N + EA\varepsilon)\delta\varepsilon + N_x\delta u + \left(-\varepsilon_o + u_x + \frac{1}{2}{v_x}^2\right)\delta N\, dx - (Q - Q_{int})^T\delta q \qquad \textbf{(55)}$$

Implementation of the stationary condition $\delta\Pi_{VHW} = 0$ along with the fundamental lemma of the calculus of variations, derives the whole mathematical description of the problem. In other words the VHW principle encpsulates all the essential information for the solution, i.e.:

- Constitutive relations
- Equations of equilibrium

- Kinematic relations
- Natural boundary conditions

If constitutive relations of the cross sections are inserted in **(54)**, then the Hellinger – Reissner functional is derived:

$$\Pi_{HR}(v,u,N,M) = \frac{1}{2}\int_0^l \left(\frac{N^2}{EA} + \frac{M^2}{EI}\right) dx + \int_0^l \left(-\frac{N}{EA} + u_x + \frac{1}{2}{v_x}^2\right) N\, dx$$

$$\int_0^l \left(+\frac{M}{EI} - v_{xx}\right) M\, dx - Q^T q \;\Leftrightarrow$$

$$\Pi_{HR}(v,u,N,M) = \int_0^l \left[N\left(u_x + \frac{1}{2}{v_x}^2\right) - \frac{N^2}{2EA}\right] dx + \int_0^l \left(M v_{xx} - \frac{M^2}{2EA}\right) dx - Q^T q \quad \textbf{(56)}$$

Furthermore, if we eliminate also the displacements via the cross sectional constitutive relations, yields:

$$\Pi_{TCPE}(v,u,N,M) = \frac{1}{2}\int_0^l \left(\frac{N^2}{EA} + \frac{M^2}{EI}\right) dx - Q^T q \quad \textbf{(57)}$$

which is the single – field Total Complementary Potential Energy functional (TCPE). Notice that all the different expressions presented above emanate from the general three – field VHW functional.

3.3 Fiber Beam – Column Finite Element Formulations

Finite Element formulation is based on the variational principle $\delta\Pi = 0$. This is the starting point for developing every type of finite element (displacement based, force based, mixed). The difference among these types lies on which functional is selected and subsequently what shape functions are introduced for the varied quantities. This process is the same for beam – column, plate, shell, plane stress, plane strain or hexahedral finite elements, however each one keeps its special features.

Within the beam – column formulation, necessity of integrating stresses over the cross section area emerges during the analysis. That is essential for the determination of stress resultants (bending moments, normal forces) which are of major importance in engineering practice.

Integration can be carried out either by a Gaussian scheme or by a discretization of the cross section into uniaxial fibers. The second concept delimits a special category of beam – column finite elements; the *fiber beam – column elements*.

In the case of small displacements from $\delta \Pi_{TPE} = 0$ we derive the variational principle:

$$\int_0^l \delta d^T \cdot k \cdot d \, dx - \delta q^T Q = 0 \tag{58}$$

where $D^T = [M \quad N]$ and $d^T = [\kappa \quad \varepsilon_o]$ and k is the cross section stiffness matrix which due to the fiber discretization is written as:

$$k = \begin{bmatrix} \sum E_i A_i & -\sum E_i A_i \, y_i \\ -\sum E_i A_i \, y_i & \sum E_i A_i \, {y_i}^2 \end{bmatrix} \tag{59}$$

where index $i = 1, \dots, n_f$ refers to the respective fiber and n_f is the number of fibers. Considering the standard cubic shape functions for the interpolation of the displacement field we obtain the equation:

$$\left(\int_0^l a^T \cdot k \cdot a \, dx \right) \cdot q - Q = 0 \tag{60}$$

where $\int_0^l a^T \cdot k \cdot a \, dx = K$ is the element stiffness matrix. The matrix $a(x)$ is termed as the strain matrix, because its product with nodal displacements q defines the strain field d along the element:

$$\boldsymbol{a}(x) = \begin{bmatrix} -\frac{1}{l} & 0 & 0 & \frac{1}{l} & 0 & 0 \\ 0 & -\frac{6}{l^2}+\frac{12x}{l^3} & -\frac{4}{l}+\frac{6x}{l^2} & 0 & \frac{6}{l^2}-\frac{12x}{l^3} & -\frac{2}{l}+\frac{6x}{l^2} \end{bmatrix} \quad \textbf{(61)}$$

$$d(x) = a(x) \cdot q \quad \textbf{(62)}$$

The above procedure describes the concept of displacement based fiber beam – column elements. For the formulation of the force based elements the shape functions interpolate the field of stress resultants. Thus:

$$b = \begin{bmatrix} 1 & -\frac{x}{l} & \frac{x}{l} & 0 \\ 0 & 0 & 0 & 1 \end{bmatrix} \quad \textbf{(63)}$$

$$D(x) = b(x) \cdot Q_n \quad \textbf{(64)}$$

where index N are the designates the natural (or corrotational) system where rigid body motion has been eliminated via the transformation:

$$Q = B^T \cdot Q_N \ , q_N = B \cdot q \quad \textbf{(65)}$$

$$[B] = \begin{bmatrix} 0 & \frac{1}{l} & 0 & 0 & -\frac{1}{l} & 0 \\ 0 & \frac{1}{l} & 0 & 0 & -\frac{1}{l} & 0 \\ 1 & 0 & 0 & -1 & 0 & 1 \end{bmatrix} \quad \textbf{(66)}$$

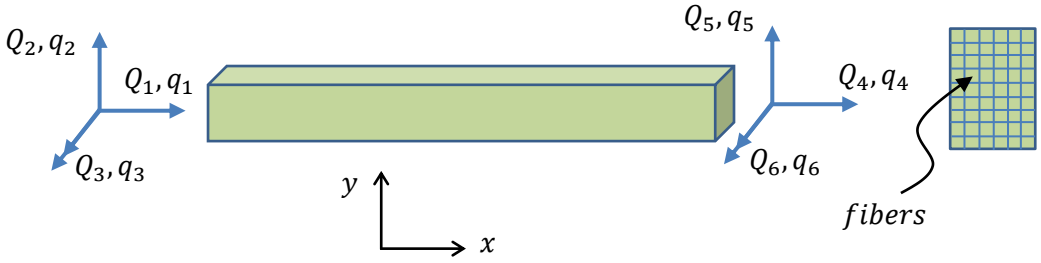

Figure 10: Fiber beam – column element in local coordinate system

Using the stationary point of the TCPE potential we obtain, the principal of virtual forces:

$$\int_0^l \delta D^T \cdot k^{-1} \cdot D \, dx - \delta {Q_N}^T q_N = 0 \Leftrightarrow$$

$$\int_0^l b^T \cdot k^{-1} \cdot b \, dx - q_N = 0 \tag{67}$$

where $\int_0^l b^T \cdot k^{-1} \cdot b \, dx = F$ is the element flexibility matrix. These two basic formulations presented about, namely the displacement and the force based approach, coincide if we assume small displacements and elastic materials, however in general $K^{-1} \neq F$.

Various fiber beam – column elements have been developed and proposed within the theory of large displacements. Overall it is pointed out that displacement based elements, which are driven by the classical concept of the finite element formulation based on the stationary of TPE (principle of virtual work), have been replaced by force based and mixed fiber elements. This holds because displacement elements increase the discretization required for realistic analysis results, as they satisfy equilibrium in an average sense. On the other hand, force based elements satisfy equilibrium and thus do not require a fine

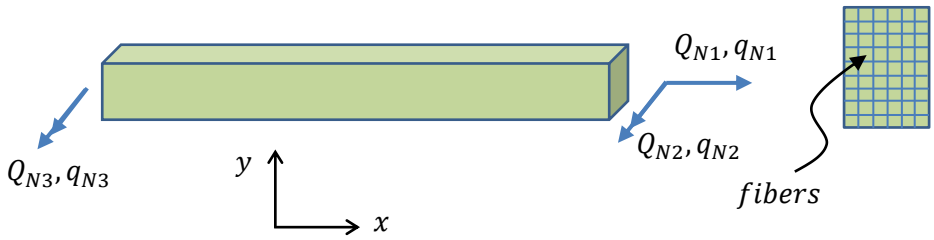

Figure 11: Fiber beam – column element in natural system

discretization. However in nonlinear problems force based elements violate compatibility (or even better satisfy compatibility in an average way), thus either additional iterations must be enforced in the solution algorithm, or one should pursuit a solution within mixed elements that handle the violation of compatibility.

If large displacements and moderate rotations are taken into account the interpolation matrix b of the force based formulation can be modified as follows:

$$b = \begin{bmatrix} 1 - \frac{x}{l} & \frac{x}{l} & v(x) \\ 0 & 0 & 1 \end{bmatrix} \quad \textbf{(68)}$$

Shape functions **(68)** of the stress resultants can be immediately derived by equations **(53)** presented in the previous section. This modification of b implies that the displacement field within the element should be defined, being though unknown in the force based approach. This problem was effectively treated by Neuenhofer and Filippou (1998), who developed a Curvature Based Displacement Interpolation (CBDI). In the CBDI procedure, the curvature field is approximated using Lagrange polynomials and then integrated to find the transverse displacement field. However, despite the fact that this approach maintains the benefits of the force based elements, it also adopts simplified expressions for curvature and axial deformation, thus demands a finer discretization in highly geometrically nonlinear problems. This aspect is examined in detail in section 5.

In Neuenhofer and Filippou (1998) the geometrical nonlinearity of the force based element was introduced via the HR potential, which can be expressed also in the following compact form:

$$\Pi_{HR}(D,u) = \int_0^l \left(D^T \cdot \begin{Bmatrix} v_{xx} \\ u_x + \frac{1}{2} {v_x}^2 \end{Bmatrix} - W_c^{(A)}(D) \right) dx - Q^T q \quad \textbf{(69)}$$

where $W_c^{(A)}(D)$ is the complementary energy density in terms of the stress resultants D:

$$W_c^{(A)}(D) = \iint_A W_c(\sigma)\, dA \quad \textbf{(70)}$$

In accordance with equation **(46)** we can state for the stress resultants and deformations $(M, N, \kappa, \varepsilon_o)$ a similar equation:

$$W^{(A)}(d) + W_c^{(A)}(D) = D^T \cdot d \quad \textbf{(71)}$$

Implementing the stationary condition of the HR potential **(56)** $\delta\Pi_{HR}(D,u) = 0$, we obtain:

$$\delta\Pi_{HR}(D,u) = \int_0^l D^T \cdot \begin{Bmatrix} \delta v_{xx} \\ \delta u_x + v_x \delta u_x \end{Bmatrix} dx$$

$$+ \int_0^l \delta D^T \cdot \left(\begin{Bmatrix} v_{xx} \\ u_x + \frac{1}{2} {v_x}^2 \end{Bmatrix} - d \right) dx - {Q_N}^T \delta q_N = 0 \qquad \textbf{(72)}$$

which is equivalent to :

$$\delta_u \Pi_{HR} + \delta_D \Pi_{HR} = 0 \Rightarrow \begin{matrix} \delta_u \Pi_{HR} = \int_0^l D^T \cdot \begin{Bmatrix} \delta v_{xx} \\ \delta u_x + v_x \delta u_x \end{Bmatrix} dx - Q^T \delta q = 0 \\ \delta_D \Pi_{HR} = \int_0^l \delta D^T \cdot \left(\begin{Bmatrix} v_{xx} \\ u_x + \frac{1}{2} {v_x}^2 \end{Bmatrix} - d \right) dx = 0 \end{matrix} \qquad \textbf{(73)}$$

The first relation leads to the differential equation **(53)**, which shows the way for choosing the shape functions **(68)** for the interpolation of the stress resultants field. The second equation after some integrations by parts, yields:

$$\int_0^l \left[\delta N_x u + \left(\frac{1}{2} \frac{d(\delta N v_x)}{dx} - \delta M_{xx} \right) v + \delta N \varepsilon_o + \delta M \kappa \right] dx - \delta N(l) u(l)$$

$$- [\delta M(x) v_x(x)]_0^l = 0 \qquad \textbf{(74)}$$

In order to enforce a stationary point of the HR potential, the first two terms of this equation are set equal to zero for non – zero displacements *u* and *v*, hence the following relations are derived:

$$\delta N_x = 0$$

$$\frac{1}{2} \frac{d(\delta N v_x)}{dx} - \delta M_{xx} = 0 \qquad \textbf{(75)}$$

Interpolation over the virtual field of the stress resultants, results from the above two equations:

$$\delta D = \tilde{b} \cdot \delta Q_N \tag{76}$$

$$\tilde{b} = \begin{bmatrix} 1 - \frac{x}{l} & \frac{x}{l} & \frac{1}{2}v(x) \\ 0 & 0 & 1 \end{bmatrix} \tag{77}$$

Subsequently, we substitute equations **(76)** and **(75)** into **(74)** to obtain the integral of the nodal displacements:

$$q_N = \int_0^l \tilde{b}^T \cdot d \, dx \tag{78}$$

This equation implies that the consistent flexibility matrix is not symmetric:

$$F = \frac{\partial q_N}{\partial Q_N} = \int_0^l \left[\tilde{b}^T(x) \cdot k^{-1}(x)[b(x) + h(x)] + g(x)\right] dx \tag{79}$$

$$h(x) = \frac{\partial b(x)}{\partial v(x)} Q_N \frac{\partial v(x)}{\partial Q_N}$$

$$g(x) = \frac{\partial \tilde{b}(x)^T}{\partial v(x)} d(x) \frac{\partial v(x)}{\partial Q_N} \tag{80}$$

The partial derivative $\frac{\partial v(x)}{\partial Q_N}$ is evaluated via the CBDI procedure for every individual $\frac{\partial v_i}{\partial Q_N}$ that appears in the integration scheme implemented for the calculation of the integral **(79)**. It should be underlined that the Gauss-Legendre quadrature is the only approach that guarantees symmetry of the element flexibility matrix (De Souza 2000).

4 Primal – Dual Methods for a New Beam-Colum Element

Optimization is widely used in structural design, providing engineers with a powerful tool for determining the optimum relation among safety, serviceability and cost. Apart from this, optimization algorithms stand in the core of direct methods of limit analysis, allowing for the direct calculation of the collapse load factor of a structure taking into account the evolution of plastic deformations. However the results coming out of the direct methods have a major drawback; they lack of essential information at the intermediate steps along the equilibrium paths, thus obtaining just a single value of the critical load factor. Moreover the extension of limit analysis to large displacement problems has not been yet fully addressed.

As presented in the previous chapter, FEM formulation is based on the idea of finding a stationary point of a potential, i.e. a vector of varying quantities minimizing this potential. However, in most formulations we enforce a solution of the minimization problem by foretelling the evolution of the included fields. In general these fields, interpolated by custom shape functions, do not coincide with the real ones and hence, an inherent error is introduced into the final results in relation to real response.

This chapter focuses on a straight forward solution process of the minimization problem, which uses a curvature based interpolation for $\theta(x)$ and avoids further limitations introduced by corrotational transformation. Since there are no restrictions to the rotation magnitude, implied by corrotational formulations, this element accounts for arbitrary large rotations. Finally, the proposed formulation obtains a *hybrid – type beam – column element* whose only approximation relates to the $\theta -$ interpolation and the integration scheme.

The element is suitable for problems accounting for geometrical and material nonlinearities within the Euler – Bernoulli beam theory. For the calculation of cross sectional forces the concept of fiber discretization is adopted, in which each fiber exhibits a uniaxial behavior

under the constraint of plane sections which remain plane and perpendicular to the curved axis.

4.1 Newton – Raphson Formulation

In order to formulate the minimization problem we need to determine the variables, the objective function and the constraints. Once these are specified, Lagrange multipliers are introduced to build the augmented potential. Finally the integrals that appear in the generalized relation are expressed via a Gaussian quadrature scheme and thus the minimization of a functional reduces to the minimization of a function.

4.1.1 Elemental level

For the objective function Π the summation of internal energy U of the element together with external work Ω is chosen. Internal energy, either stored or dissipated as elastic or plastic energy respectively, is expressed in terms of total deformation $d = [\kappa, \varepsilon_o]^T$, while external work is defined as the work of external forces $\bar{Q}$ in terms of nodal displacements $\bar{q}$.

$$\begin{matrix} U = \int_0^l W^{(A)}(d)\, dx \\ \Omega = -\bar{Q}^T \cdot \bar{q} \end{matrix} \Rightarrow \Pi = U + \Omega \qquad \textbf{(81)}$$

Thus the objective function Π can be rewritten in the following expanded form:

$$\Pi = \int_0^l W^{(A)}(\kappa, \varepsilon_o)\, dx - \bar{Q}^T \cdot \bar{q} \qquad \textbf{(82)}$$

Notice that the potential above is a function of nodal displacements $\bar{q}$ in the global coordinate system and deformation fields $\kappa(x), \varepsilon_o(x)$.

The constraints of the problem account for the kinematic relations. In other words, what is not fulfilled by the unconstrained minimization expression **(82)** is compatibility, which must be imposed via equality constraints. According to relations **(38)**, deformations and displacements of each element i must satisfy three equations:

$$q_4 - q_1 = \int_0^l [(\varepsilon_o + 1) \cdot cos\theta - 1]\, dx$$

$$q_5 - q_2 = \int_0^l (\varepsilon_o + 1) \cdot sin\theta\, dx \qquad \textbf{(83)}$$

$$q_6 - q_3 = \int_0^l \kappa\, dx$$

The above constraints will be denoted as $\boldsymbol{h} = \mathbf{0}$. The integrals of the above equations are evaluated via the Gauss – Legendre quadrature. Equations above can be casted into matrix form as:

$$B \cdot \bar{q} = L^T \cdot \int_0^l \Phi\, dx \approx L^T \cdot \sum_{i=1}^{n} \frac{l}{2} w_i \Phi_i \qquad \textbf{(84)}$$

where n is the number of the integration points and:

$$B = \begin{bmatrix} -1 & 0 & 0 & 1 & 0 & 0 \\ 0 & -1 & 0 & 0 & 1 & 0 \\ 0 & 0 & -1 & 0 & 0 & 1 \end{bmatrix} \qquad \textbf{(85)}$$

$$L = \begin{bmatrix} cos\varphi & sin\varphi & 0 \\ -sin\varphi & cos\varphi & 0 \\ 0 & 0 & 1 \end{bmatrix} \qquad \textbf{(86)}$$

$$\Phi = \begin{bmatrix} (\varepsilon_o + 1)cos\theta - 1 \\ (\varepsilon_o + 1)sin\theta \\ \kappa \end{bmatrix} \qquad \textbf{(87)}$$

$$\theta(x) = \bar{q}_3 + \int_0^x \kappa(\tau)\, d\tau \qquad \textbf{(88)}$$

Introducing Lagrange multipliers λ we can derive a generalized form of potential **(82)**, using also relation **(83)**:

$$f = \int_0^l W^{(A)}(d)\, dx - \bar{Q}^T \cdot \bar{q} + \lambda^T \left(B \cdot \bar{q} - L^T \cdot \int_0^l \Phi\, dx \right) \qquad \textbf{(89)}$$

The first variation of the generalized potential is written as follows:

$$\delta f = 0 \Rightarrow \begin{matrix} \delta_d f = 0 \\ \delta_{\bar{q}} f = 0 \\ \delta_\lambda f = 0 \end{matrix} \Longrightarrow$$

$$\begin{matrix} \int_0^l D(x)^T\, \delta d\, dx - \lambda^T L^T \cdot \int_0^l \frac{\partial \Phi}{\partial d}\, \delta d\, dx = 0 \\ \left(-\bar{Q}^T + \lambda^T B - \lambda^T L^T \cdot \int_0^l \frac{\partial \Phi}{\partial \bar{q}}\, dx \right) \delta \bar{q} = 0 \\ \delta \lambda^T \left(B \cdot \bar{q} - L^T \cdot \int_0^l \Phi\, dx \right) = 0 \end{matrix} \Rightarrow \begin{matrix} D(x)^T - \lambda^T L^T \cdot \frac{\partial \Phi}{\partial d} = 0 \\ -\bar{Q}^T + \lambda^T B - \lambda^T L^T \cdot \int_0^l \frac{\partial \Phi}{\partial \bar{q}}\, dx \\ B \cdot \bar{q} - L^T \cdot \int_0^l \Phi\, dx \end{matrix} \quad \textbf{(90)}$$

where the first equation **(90)** governs equilibrium within the element, the second expresses the nodal equilibrium and the third the nodal compatibility. As mentioned before integral $\int_0^l \Phi\, dx$ is evaluated via the Gauss – Legendre quadrature, thus the set of equations **(90)** yields:

$$\begin{matrix} \int_0^l D(x)^T\, \delta d\, dx - \lambda^T L^T \cdot \sum_{i=1}^{n} \sum_{j=1}^{n} \frac{l}{2} w_j \frac{\partial \Phi_j}{\partial \{d_i\}}\, \delta \{d_i\} = 0 \\ \left(-\bar{Q}^T + \lambda^T B - \lambda^T L^T \cdot \sum_{i=1}^{n} \frac{l}{2} w_i \frac{\partial \Phi_i}{\partial \bar{q}} \right) \delta \bar{q} = 0 \\ \delta \lambda^T \left(B \cdot \bar{q} - L^T \cdot \sum_{i=1}^{n} \frac{l}{2} w_i \Phi_i \right) = 0 \end{matrix} \quad \textbf{(91)}$$

where $\{d_i\}^T = \{\kappa_i \quad \varepsilon_i\}$. By transposing the second equation of set **(91)** we can derive the following expression of the Lagrange multipliers and nodal forces:

$$\bar{Q} = T \cdot \lambda \quad \textbf{(92)}$$

where,

$$T = B^T - \sum_{i=1}^{n} \frac{l}{2} w_i \frac{\partial \Phi_i}{\partial \bar{q}} \cdot L \quad \textbf{(93)}$$

At this point the interpolation of the strain field is introduced in order to exploit the weighted integral of equation **(90)**. It should be noticed that the interpolation of the strain field is developed based on the n Gauss – Legendre points used for the evaluation of integrals in **(91)**. Thus:

$$\begin{bmatrix}\kappa(x)\\ \varepsilon(x)\end{bmatrix} = \sum_{i=1}^{n} N_i(x) \cdot \begin{bmatrix}\kappa_i\\ \varepsilon_i\end{bmatrix} \tag{94}$$

where $l_i(x)$ are the Lagrange polynomials which are expressed as follows:

$$N_i(\xi) = \frac{\prod_{j=1}^{n}(\xi - \xi_j)}{\prod_{j=1, j\neq i}^{n}(\xi_i - \xi_j)}, \xi = \frac{x}{l} \tag{95}$$

In pure matrix notation we can rewrite relation **(94)** as:

$$d = N \cdot \{d\} \tag{96}$$

where $\{d\}^T = [\{\kappa_1 \quad \varepsilon_1\} \quad ... \quad \{\kappa_n \quad \varepsilon_n\}]$ and $N^T = [N_1 \quad ... \quad N_n]$. Equation **(90)** now yields:

$$\int_0^l D(x)^T N_i dx - \lambda^T L^T \cdot \sum_{j=1}^{n}\left(\frac{l}{2} w_j \frac{\partial \Phi_j}{\partial\{d_i\}}\right) = 0 \tag{97}$$

which stands for every $i = 1, \dots, n$. Using the same integration scheme with the same number of points for the evaluation of $\int_0^l {N_i}^T D(x)\, dx$, equation **(97)** reduces to:

$$w_i D(x_i)^T - \lambda^T L^T \cdot \sum_{j=1}^{n}\left(w_j \frac{\partial \Phi_j}{\partial\{d_i\}}\right) = 0 \tag{98}$$

The interpolation scheme described above can be used also to express $\theta(x)$ in terms of $\{\kappa\}$. From relations **(88)** and **(96)** we derive:

$$\theta(x) = \bar{q}_3 + \int_0^x N(\tau)\, d\tau \cdot \{\kappa\} \tag{99}$$

The Lagrange polynomials defining shape functions N can be expressed also as:

$$N(\xi) = [1 \quad \xi \quad ... \quad \xi^{n-1}] \cdot G^{-1} \tag{100}$$

where matrix G is the so – called Vandermode matrix, which is written as:

$$G = \begin{bmatrix} 1 & \xi_1 & \xi_1^2 & \dots & \xi_1^{n-1} \\ \vdots & \vdots & \vdots & \ddots & \vdots \\ 1 & \xi_n & \xi_n^2 & \dots & \xi_1^{n-1} \end{bmatrix} \quad \textbf{(101)}$$

Substituting relation **(100)** into **(99)** gives:

$$\theta(x) = \bar{q}_3 + \Theta \cdot \{\kappa\} \quad \textbf{(102)}$$

$$\Theta = l\left[\xi \quad \frac{\xi^2}{2} \quad \dots \quad \frac{\xi^n}{n}\right] \cdot G^{-1} \quad \textbf{(103)}$$

From relation **(102)** we can determine every $\theta_i = \theta(x_i)$ of the n Gauss – Legendre points. The partial derivatives appearing in equations **(91)** have the following form:

$$\frac{\partial \Phi_j}{\partial \{d_i\}}^T = \begin{bmatrix} -\Theta_{ji}(\varepsilon_{oj}+1)sin\theta_j & \Theta_{ji}(\varepsilon_{oj}+1)cos\theta_j & \delta_{ji} \\ \delta_{ji}cos\theta_j & \delta_{ji}sin\theta_j & 0 \end{bmatrix}$$

$$\frac{\partial \Phi_i}{\partial \bar{q}} = \begin{bmatrix} 0 & 0 & -(\varepsilon_{oi}+1)sin\theta_i & 0 & 0 & 0 \\ 0 & 0 & (\varepsilon_{oi}+1)cos\theta_i & 0 & 0 & 0 \\ 0 & 0 & 0 & 0 & 0 & 0 \end{bmatrix} \quad \textbf{(104)}$$

At this point the Newton – Raphson method is introduced to solve the system of equations **(91)**. As presented in paragraph 2.2.5, the iterative scheme determines the updated unknown quantities with index $k+1$ from the old ones with index k:

$$\begin{bmatrix} \nabla^2_{dd} f^k & \nabla^2_{d\bar{q}} f^k & \nabla^2_{d\lambda} f^k \\ & \nabla^2_{\bar{q}\bar{q}} f^k & \nabla^2_{\bar{q}\lambda} f^k \\ & & 0 \end{bmatrix} \cdot \begin{bmatrix} \Delta\{d\}^k \\ \Delta\bar{q}^k \\ \lambda^{k+1} \end{bmatrix} + \begin{bmatrix} \nabla_d \Pi^k \\ \nabla_{\bar{q}} \Pi^k \\ \nabla_\lambda f^k \end{bmatrix} = 0 \quad \textbf{(105)}$$

where, for δ_{ij} being the Kronecker's delta:

$$\nabla^2_{dd} f = \left[\frac{\partial^2 f}{\partial\{d_i\}\partial\{d_j\}}\right] = \left[\delta_{ij} w_i k_i - \lambda^T L^T \cdot \sum_{p=1}^{n}\left(w_p \frac{\partial^2 \Phi_p}{\partial\{d_i\}\partial\{d_j\}}\right)\right]$$

$$\nabla^2_{d\bar{q}} f = \left[\frac{\partial^2 f}{\partial\{d_i\}\partial\bar{q}_j}\right] = \left[-\lambda^T L^T \cdot \sum_{p=1}^{n}\left(w_p \frac{\partial^2 \Phi_p}{\partial\{d_i\}\partial\bar{q}_j}\right)\right] \quad \begin{matrix} if\ j=3 \\ else\ 0 \end{matrix}$$

$$\nabla^2_{d\lambda} f = \left[\frac{\partial^2 f}{\partial\{d_i\}\partial\lambda}\right] = \left[-L^T \cdot \sum_{p=1}^{n}\left(w_p \frac{\partial \Phi_p}{\partial\{d_i\}}\right)\right] \quad \textbf{(106)}$$

$$\nabla^2_{\bar{q}\bar{q}} f = \left[\frac{\partial^2 f}{\partial \bar{q}_i \partial \bar{q}_j}\right] = \begin{bmatrix} -\lambda^T L^T \cdot \sum_{p=1}^{n} \frac{l}{2} w_p \frac{\partial^2 \Phi_p}{\partial \bar{q}_i \partial \bar{q}_j} \end{bmatrix} \begin{matrix} if\ i = j = 3 \\ else\ 0 \end{matrix}$$

$$\nabla^2_{\bar{q}\lambda} f = T$$

$$\nabla_d \Pi = \{w_i D(x_i)\}$$

$$\nabla_{\bar{q}} \Pi = -\bar{Q}^T$$

$$\nabla_\lambda f = B \cdot \bar{q} - L^T \cdot \sum_{i=1}^{n} \frac{l}{2} w_i \Phi_i$$

The square matrix of equation **(105)** is the analytic Hessian matrix of the generalized potential. The partial derivatives appearing in equations **(106)** are determined as follows:

$$\frac{\partial^2 \Phi_p}{\partial\{d_i\}\partial\{d_j\}} = \Theta_{pi} \begin{bmatrix} -\Theta_{pj}(\varepsilon_{op}+1)cos\theta_p & -\delta_{pi} sin\theta_p & -\Theta_{pj}(\varepsilon_{op}+1)sin\theta_p & \delta_{pi} cos\theta_p \\ -\delta_{pi} sin\theta_p & 0 & \delta_{pi} cos\theta_p & 0 \end{bmatrix}$$

$$\frac{\partial^2 \Phi_p}{\partial\{d_i\}\partial\bar{q}} = \begin{bmatrix} & -\Theta_{pi}(\varepsilon_{op}+1)cos\theta_p & -sin\theta_p & \\ O & -\Theta_{pi}(\varepsilon_{op}+1)sin\theta_p & cos\theta_p & O \\ & 0 & 0 & \end{bmatrix}$$

$$\frac{\partial \Phi_i}{\partial \bar{q}} = \begin{bmatrix} 0 & 0 & -(\varepsilon_{oi}+1)sin\theta_i & 0 & 0 & 0 \\ 0 & 0 & (\varepsilon_{oi}+1)cos\theta_i & 0 & 0 & 0 \\ 0 & 0 & 0 & 0 & 0 & 0 \end{bmatrix} \quad \textbf{(107)}$$

$$\frac{\partial^2 \Phi_p}{\partial \bar{q} \partial \bar{q}} = \begin{bmatrix} & O & \\ O & -(\varepsilon_{op}+1)cos\theta_p & O \\ & -(\varepsilon_{op}+1)sin\theta_p & \\ & O & \end{bmatrix}$$

Hence, from the above relations we can determine the tangential Hessian matrix at iteration k:

$$H^k = \begin{bmatrix} \nabla^2_{dd} f^k & \nabla^2_{d\bar{q}} f^k & \nabla^2_{d\lambda} f^k \\ & \nabla^2_{\bar{q}\bar{q}} f^k & \nabla^2_{\bar{q}\lambda} f^k \\ & & 0 \end{bmatrix} \quad \textbf{(108)}$$

Of course, Newton – Raphson scheme can be modified by not updating **(108)** iteration upon iteration, but instead utilizing the Hessian matrix of the first iteration H^o. That certainly increases the total number of iterations required for convergence, but decreases the overall computational cost in large problems as the inverse of the hessian is calculated only once.

4.1.2 Structural level

For every element of the structure nodal displacements $\Delta\bar{q}$ coincide with some of the structural nodal displacements $\Delta\bar{u}$ (also termed as structural degrees of freedom). In order to assemble the overall structural matrices the key relation is the second relation in **(105)**, which can be rewritten for every node as:

$$\nabla^2_{\bar{q}d} f_j \cdot \Delta\{d\}_j + \nabla^2_{\bar{q}\bar{q}} f_j \cdot \Delta\bar{u}_i + \nabla^2_{\bar{q}\lambda} f_j \cdot \lambda_j = \bar{Q}^T{}_{ij} \qquad \textbf{(109)}$$

where i denotes the node number and j the element number. Index k referring to the iteration scheme has been dropped from relation **(109)** for sake of notational simplification. Summing up relations **(109)** of node i together, for all elements having i as a starting or ending point, we obtain:

$$\sum \nabla^2_{\bar{q}d} f_j \cdot \Delta\{d\}_j + \cdot \left(\sum \nabla^2_{\bar{q}\bar{q}} f_j \right) \Delta\bar{u}_i + \sum \nabla^2_{\bar{q}\lambda} f_j \cdot \lambda_j = P_i \qquad \textbf{(110)}$$

where P_i are the external forces of structural node i. Relation **(110)** can be expressed in a more compact form for all structural degrees of freedom by introducing the Boolean matrices $t_d, t_{\bar{q}}, t_\lambda$:

$$\left(\sum_{j=1}^{n_{el}} t_{\bar{q}j}{}^T \nabla^2_{\bar{q}d} f_j \; t_{dj} \right) \Delta\{d\}_s + \left(\sum_{j=1}^{n_{el}} t_{\bar{q}j}{}^T \nabla^2_{\bar{q}\bar{q}} f_j \; t_{\bar{q}j} \right) \Delta\bar{u} + \left(\sum_{j=1}^{n_{el}} t_{\bar{q}j}{}^T \nabla^2_{\bar{q}\lambda} f \; t_{\lambda j} \right) \lambda_s = P \qquad \textbf{(111)}$$

where $\{d\}_s, \lambda_s$ comprise all deformations and Lagrange multipliers of the structure (rows of $(2n \cdot n_{el}$ x 1) and ($3n_{el}$ x 1) respectively) and $t_d, t_{\bar{q}}, t_\lambda$ are defined as follows:

$$\begin{aligned} \Delta\bar{q}_j &= t_{\bar{q}j} \, \Delta\bar{u} \\ \Delta\{d\}_j &= t_{dj} \, \Delta\{d\}_s \\ \lambda_j &= t_{\lambda j} \, \lambda_s \end{aligned} \qquad \textbf{(112)}$$

The first equation is written in an analogous form for every element j as:

$$\left(\sum_{j=1}^{n_{el}} {t_{dj}}^T \nabla^2_{dd} f\ t_{dj}\right) \Delta\{d\}_s + \left(\sum_{j=1}^{n_{el}} {t_{dj}}^T\ \nabla^2_{d\bar{q}} f_j\ t_{\bar{q}j}\right) \Delta\bar{u} + \left(\sum_{j=1}^{n_{el}} {t_{dj}}^T\ \nabla^2_{d\lambda} f_j\ t_{\lambda j}\right) \lambda_s = \nabla_d \Pi_s \quad \textbf{(113)}$$

where in matrix $\nabla_d \Pi$ all the weighted stress resultants of the structure are sorted in a same sense as in the sixth of relations **(106)**. For notational convenience we designate $\nabla_d \Pi_s = \{\nabla_d \Pi_j\}$. Finally the third equation of **(105)** results:

$$\left(\sum_{j=1}^{n_{el}} {t_{dj}}^T \nabla^2_{d\lambda} f\ t_{dj}\right) \Delta\{d\}_s + \left(\sum_{j=1}^{n_{el}} {t_{dj}}^T\ \nabla^2_{\bar{q}\lambda} f_j\ t_{\bar{q}j}\right) \Delta\bar{u} = \nabla_\lambda f_s \quad \textbf{(114)}$$

where $\nabla_\lambda f_s = \{\nabla_\lambda f_j\}$ sorts all compatibility residuals. Hence, from relations **(111)**, **(113)** and **(114)** of the above formulation we can derive the final Newton – Raphson equation of the overall structure.

4.2 Arc – Length Formulation

In geometrical nonlinear analysis of structures an arc – length technique should be addressed thoroughly. Arc – Length numerical scheme which was originally proposed by Riks (1979) and further developed by Crisfield (1981). It allows for the detailed derivation of equilibrium paths even if snap – throughs or snap – backs are included. In other words Arc – Length is capable of overpassing singular points of stiffness or flexibility, thus, being a valuable numerical tool for nonlinear analysis of structures.

Consider that we have derived the analytic Hessian matrix of the entire structure in the increment k, H_s^k, as determined in the previous section. Let us use operator δ instead of Δ for notational convenience to represent the increments. Operator Δ herein denotes the cumulative quantities within the step. Then we can write the linearized equation of the stationary point as:

$$H_s^k \cdot \delta y^k = p^{k+1} \cdot \nabla F_{ex} - \nabla F_{in}^k \quad \textbf{(115)}$$

where matrices $\delta y^k, \nabla F_{ex}, \nabla F_{in}^k$ are defined as follows:

$$\delta y^k = \left[\delta\{d\}_s{}^k \quad \delta\bar{u}^k \quad \delta{\lambda_s}^k\right]^T \quad \textbf{(116)}$$

(117)

$$\nabla F_{ex} = [0 \quad \hat{P} \quad 0]^T$$
$$\nabla F_{in}^k = [\nabla_d f_s^k \quad \nabla_{\bar{u}} h_s^k \cdot \lambda_s^k \quad \nabla_\lambda f_s^k]^T \qquad \textbf{(118)}$$

where $\nabla_d f_s^k, \nabla_{\bar{u}} h_s^k, \nabla_\lambda f_s^k$ are determine by a procedure exactly analogous to the one presented in paragraph 4.1.2. In equation **(115)** p is considered to be the load factor while $\hat{P}$ in equation **(117)** is a fixed external load. In order to derive the iterative procedure of arc – length method a predefined or a step – by – step updating radius of a generalized sphere or cylinder has to be defined, which herein is designated as R.

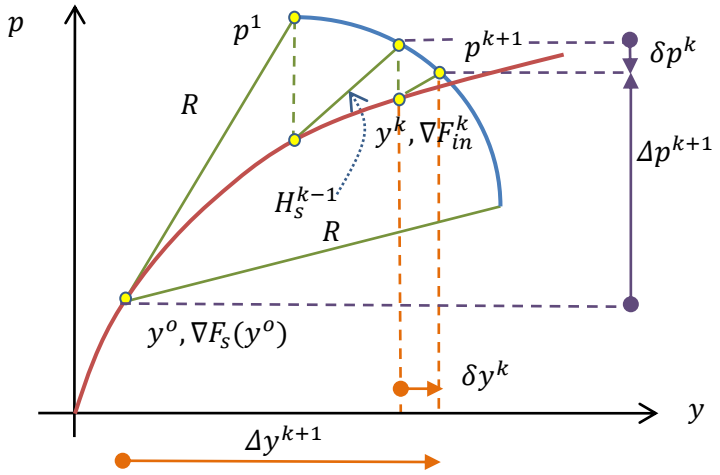

Figure 12: Arc – length method

This sphere or cylinder defining spherical and cylindrical arc – length methods respectively, acts as a constraint to the standard Newton – Raphson method, as presented in Figure 12. As also depicted in Figure 12 we introduce the following cumulative quantities:

$$\Delta y^{k+1} = \Delta y^k + \delta y^k$$
$$\Delta p^{k+1} = \Delta p^k + \delta p^k \qquad \textbf{(119)}$$
$$p^{k+1} = p^k + \delta p^k = p^o + \Delta p^k$$

Based on the above we can write for iteration k:

$$R^2 = \left(\Delta y^{k+1}\right)^T \Delta y^{k+1} + \psi^2 \left(\Delta p^{k+1}\right)^2 \left(\nabla F_{ex}{}^T \cdot \nabla F_{ex}\right) =$$

$$\left(\Delta y^k + \delta y^k\right)^T \left(\Delta y^k + \delta y^k\right) + \psi^2 \left(\Delta p^k + \delta p^k\right)^2 \left(\nabla {F_{ex}}^T \cdot \nabla F_{ex}\right) \quad \textbf{(120)}$$

Constant ψ varies from zero to unity representing cylindrical and spherical arc – length respectively. In the present work the first type of the method is adopted, thus $\psi = 0$. Substituting the two first equations of **(119)** into **(120**) we derive a quadratic equation for increment δp^k:

$$a_1 \left(\delta p^k\right)^2 + \alpha_2 \delta p^k + \alpha_3 = 0 \quad \textbf{(121)}$$

where,

$$\begin{aligned} a_1 &= \left(\delta y_{ex}^k\right)^T \delta y_{ex}^k \\ \alpha_2 &= 2(\Delta y^k + \delta y_{in}^k)^T \delta y_{ex}^k \\ \alpha_3 &= \left(\Delta y^k + \delta y_{in}^k\right)^T \left(\Delta y^k + \delta y_{in}^k\right) - R^2 \end{aligned} \quad \textbf{(122)}$$

and also,

$$\delta y_{in}^k = -\left(H_s^k\right)^{-1} \nabla F_{in}^k \quad \textbf{(123)}$$

$$\delta y_{ex}^k = \left(H_s^k\right)^{-1} \nabla F_{ex} \quad \textbf{(124)}$$

The two roots of this scalar quadratic equation will be designated δp_1^k and δp_2^k. To avoid "doubling back" on the original path, we select the root that minimizes "angle" γ:

$$cos\gamma = \frac{\left(\Delta y_1^{k+1}\right)^T \Delta y^k}{R^2} \;\; or \;\; cos\gamma = \frac{\left(\Delta y_2^{k+1}\right)^T \Delta y^k}{R^2} \quad \textbf{(125)}$$

where Δy_1^{k+1} and Δy_2^{k+1} represent the results derived by equation **(119)** when load factor p^{k+1} is calculated via δp_1^k and δp_2^k respectively. It is underlined that the algorithm is much more robust if the displacement part of the increments is introduced in relations **(120)** – **(125)**.

5 Examples and Verification

In this chapter the accuracy and reliability of the proposed element is examined. We present a set of well – known and thoroughly discussed examples of the literature and briefly investigate their special features. Subsequently, comparisons with the elements used by reputable structural analysis software (OpenSees and SeismStruct) are demonstrated in order to enhance the verification and validation process.

As mentioned before, on the basis of the proposed element, a nonlinear analysis program called NAFS (Nonlinear Analysis of Frame Structures) was developed. This software is for planar frame structures incorporating both Newton – Raphson and Arc – Length numerical schemes along with their modified versions.

In each example the scheme was selected in relation to the problem's special features. Also, except for the comparisons performed for the validation of the proposed element, figures from NAFS's interface demonstrating the deformed shape of the structures are included. In addition all the diagrams represent an equilibrium path with respect to the load factor and the displacements of the node lying right below the load. The different analyses were performed for five or eight control section (integration points), depending on the improved accuracy.

5.1 Cantilever beam with vertical load at the tip

The first example is a cantilever imposed into an incremental vertical load at the free edge (Figure 13). For this problem in the literature there exist; an analytical solution by Frish – Fay (1962), a semi – analytical solution derived by Lo and Das Gupta (1978) and a displacement based finite element solution obtained by Chan (1988). The particular feature of this problem is that as force *P* increases the nonlinear solution deviates considerably from the linear one, as the increase of the rotation at the edge cross section activates increased axial resistance. Hence, the axial stiffness gradually increases affecting the initially pure bending stiffness.

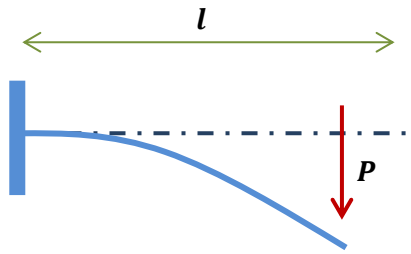

Figure 13: Cantilever under vertical tip load

Table 2: Cantilever Properties

Length, $\boldsymbol{l}$	500.0 mm
Section Height, $\boldsymbol{h}$	30.0 mm
Section Width, $\boldsymbol{b}$	30.0 mm
Young Modulus, $\boldsymbol{E}$	200.0 GPa
Yield Strain, $\boldsymbol{\varepsilon_y}$	0.010 (-)

A comparison among the geometrically nonlinear force based elements of OpenSees, SeismoStruct and the proposed formulation is depicted in Figure 14. Notice that in both OpenSees and SeismoStruct analyses at least four elements are needed for the discretization of the problem to obtain accurate results. On the other hand use of the proposed element avoids discretization provided that a sufficient number of control sections is introduced (in the present example 8 control sections were considered for the three analyses).

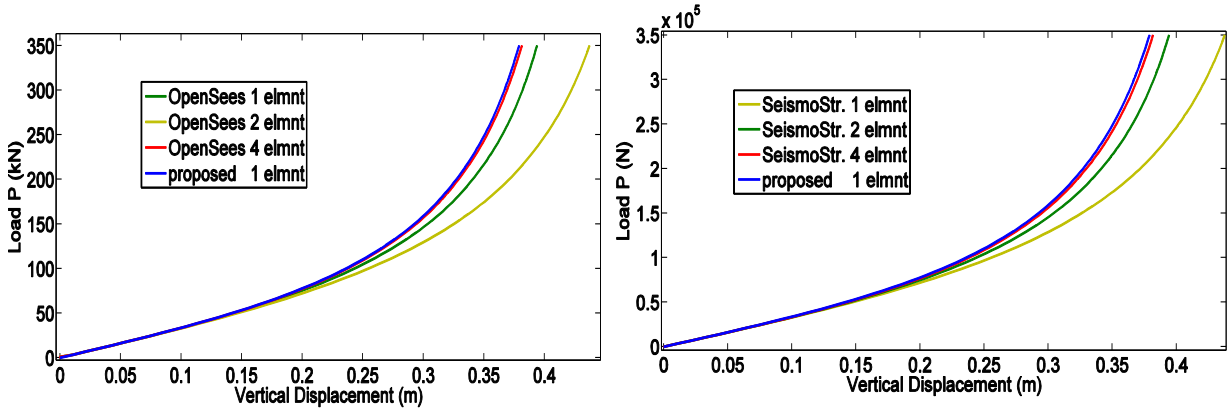

Figure 14: Equilibrium paths for different elastic analyses (free edge)

In Figure 15 the response of the element if also plasticity is taken into consideration is presented. Notice that divergence among results increases when both sources of nonlinearity, namely geometrical and material, are allowed. Hence, OpenSees accurate solution requires a finer discretization than in the elastic case (6 elements instead of 4). Analysis of SeismoStruct as also depicted in Figure 15 stopped at the load level of ~ 35 kN.

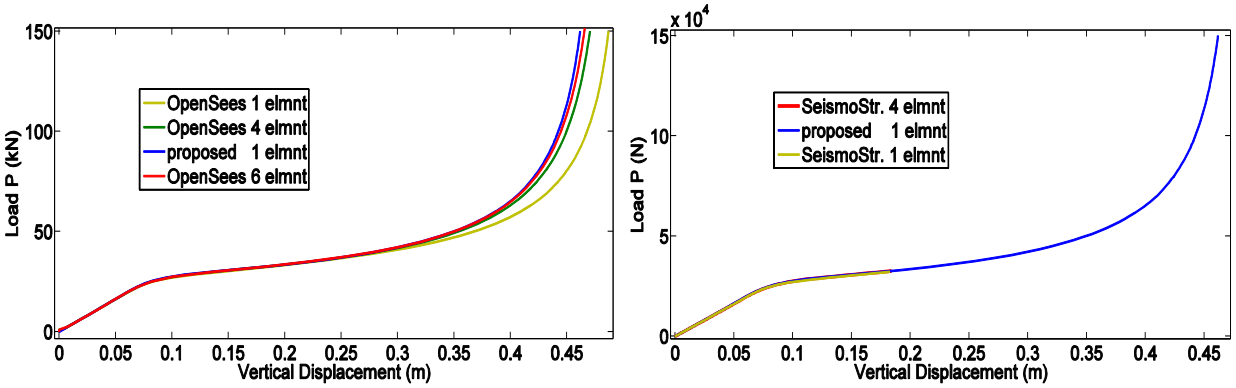

Figure 15: Equilibrium paths for different inelastic analyses (free edge)

In Figure 16 the deformed shape of the beam as obtained by NAFS's graphical interface is illustrated. In addition the final results of the Geometrically Nonlinear Elastic Analysis (GNEA) and Geometrically – Material Nonlinear Inelastic Analysis (GMNIA) using the proposed element are illustrated for comparison purpose.

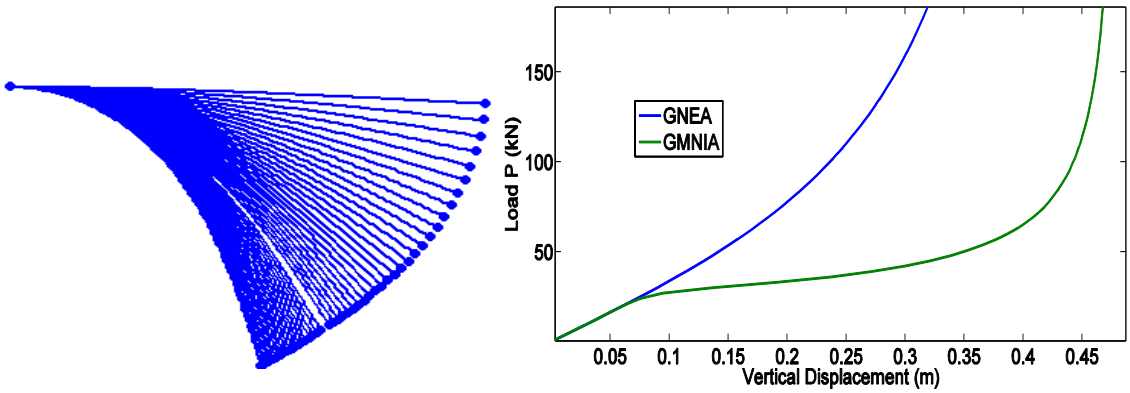

Figure 16: Deformed shape and comparison between GNEA and GMNIA

5.2 Cantilever beam with moment at the tip

Herein the same cantilever of the previous example is loaded with a concentrated moment at the free edge (Figure 17). This problem is discussed only within the elastic regime as it demonstrates some interesting features. Equilibrium at every position implies that the moment is constant within the element and thus curvature should be constant too, which means that the deformed shape is a circular arc with radius $1/\kappa$, provided that the axial deformation is

zero. The problem has been analyzed via the displacement based finite element method by Bathe and Bolourchi (1979) and Crisfield (1990) among others. Due to its unusual response as the structure exhibits really large rotations, this problem reveals all limitations and inconsistencies emanating from the different corrotational formulations.

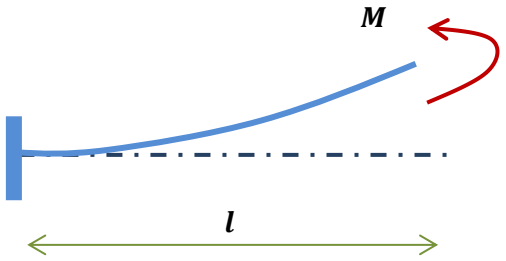

Figure 17: Cantilever with tip moment

Table 3: Cantilever Properties

Length, $\boldsymbol{l}$	500.0 mm
Section Height, $\boldsymbol{h}$	30.0 mm
Section Width, $\boldsymbol{b}$	30.0 mm
Young Modulus, $\boldsymbol{E}$	200.0 GPa
Yield Strain, $\boldsymbol{\varepsilon_y}$	(-)

Figure 18 demonstrates the results of the analysis performed using OpenSees and Seismostruct. We notice that a fine descretization (up to 5 elements) is needed by both programs in order to converge to the solution given by the proposed element. Notice also that the analysis with OpenSees stops at the load level of ~ 100 kNm. This stage represents the 90^o degree rotation of the axis related to the corotational system. Thus, the algorithm terminates because of the presence of the $arctan$ function involved in the geometrically nonlinear corotational transformation.

Analysis with the proposed element overcomes this problem as no corotational transformation is needed.

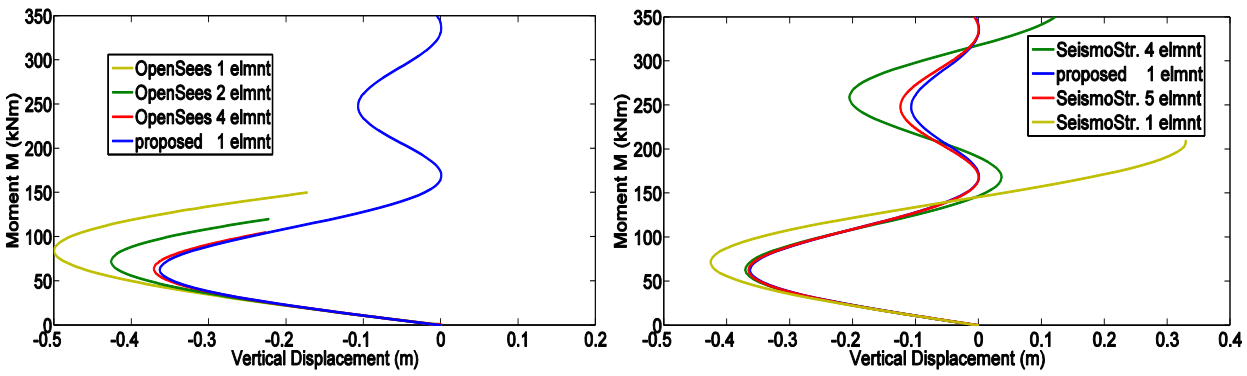

Figure 18: Equilibrium paths for different elastic analyses (free edge)

In Figure 19 the deformed shape of the beam as obtained by NAFS's graphical interface is presented. Notice that the deformed configuration coincides with a circlular arc, thus the evolution of deformation corresponds to the beam curling around itself.

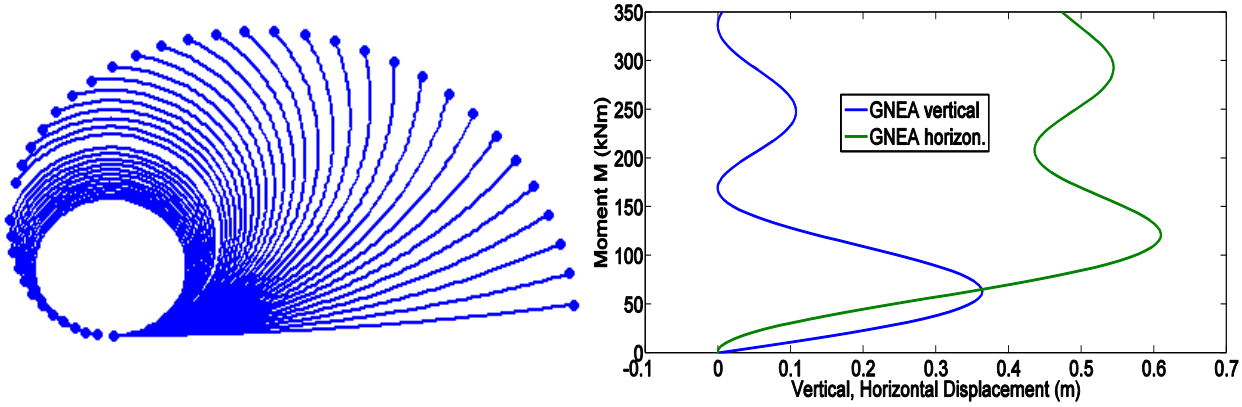

Figure 19: Deformed shape and results of GNEA

5.3 Toggle frame

This example addresses the study of a popular structure within nonlinear analysis procedures; the toggle frame (Figure 20). The geometrical properties of the toggle frame structure are shown in Table 4. This structure is usually modelled with truss elements, however herein the developed beam elements are utilized. For this problem an analytical and experimental solution has been presented by Williams (1964). Since this problem has been studied in various forms and properties by a different researchers such as Wood and Zienkiewicz (1977), Meek and Tan (1984), Chan (1988) and others, within the framework of displacement based finite elements. Chan (1988) studied the inelastic snapping behavior of the frame introducing an updated Lagrangian formulation.

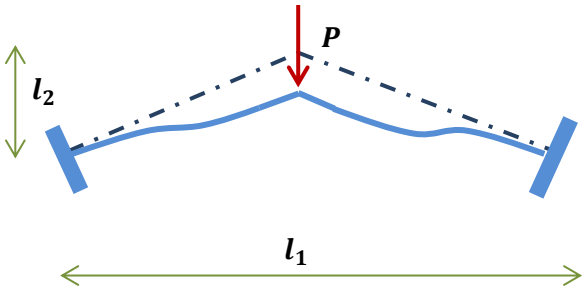

Figure 20: Toggle Frame

Table 4: Toggle Properties

Horizontal Len., l_1	2·3.00 m
Vertical Length, l_2	0.40 m
Section Height, h	300.0 mm
Section Width, b	300.0 mm
Young Modulus, E	200.0 GPa
Yield Strain, ε_y	0.01 (-)

In Figure 21 the differences among the different analyses are presented, first adapting the assumption of an elastic Hooke's material and then considering inelastic eleastoplastic behavior. For the analysis performed with OpenSees, up to 12 force based elements are required for convergence as well as for analysis with SeismoStruct. The proposed element seems to perform accurately with a coarser discretization of one element per member. The solutions based on these two codes are closer to the solution of the proposed element at relatively low load levels. For higher levels finer discretization should be implemented in order to obtain more accurate results.

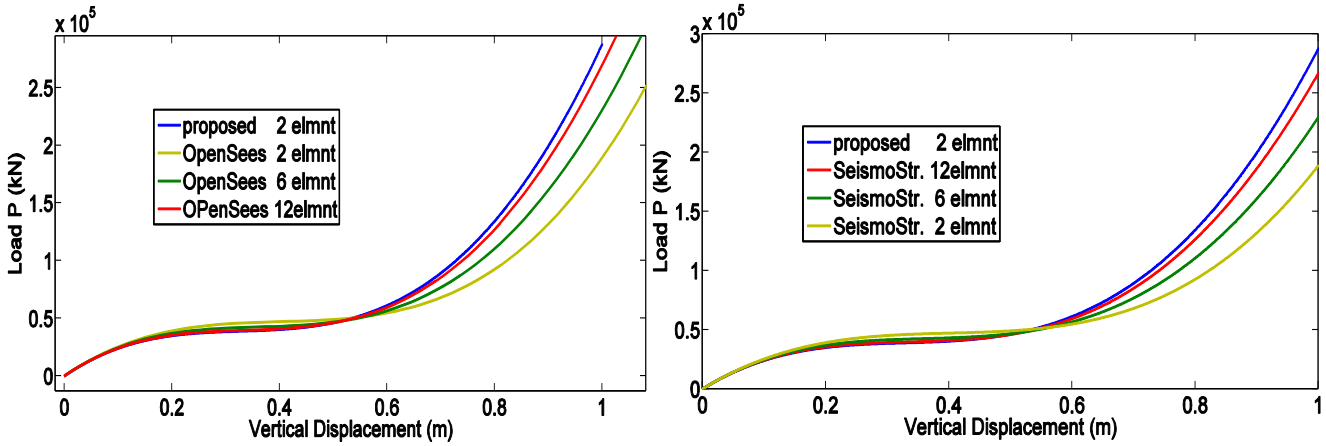

Figure 21: Equilibrium paths for different elastic analyses (top node)

In the case of elastoplastic analysis it should be noticed that the almost stable equilibrium path observed in the elastic case turns out in an unstable snap-through path as observed in Figure 22. The discretiazation needed for reliable results in OpenSees and SeismoStruct analyses shares the same features as in the elastic case, discussed above. The elastoplastic analysis with SeismoStruct stopped prematurely at the displacement level of ~ 0.35m, so only the early stages of the path that obscure snap - through were obtained.

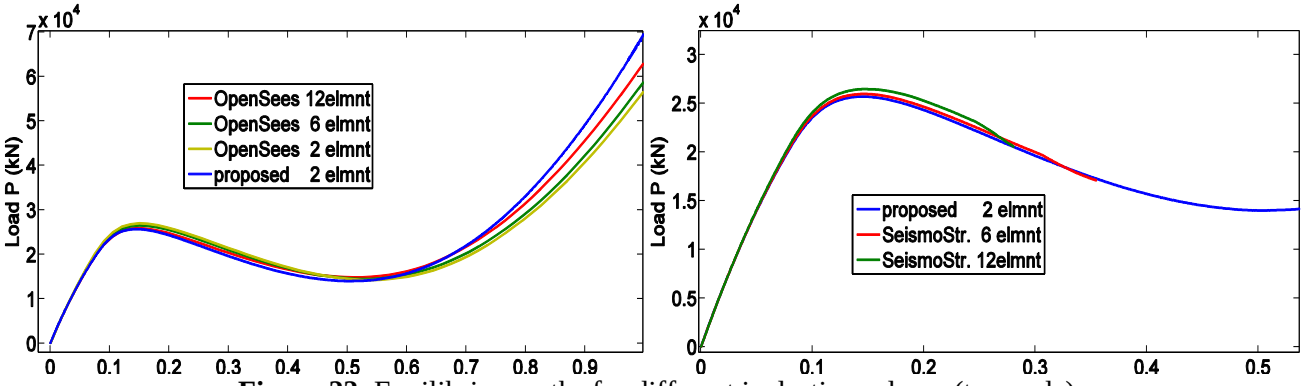

Figure 22: Equilibrium paths for different inelastic analyses (top node)

In Figure 23 the deformed shape of the toggle frame as obtained by NAFS's graphical interface is illustrated. Furthermore, the results of both the elastic and elastoplastic analyses are plotted together in order to obtain an overview of the structural response.

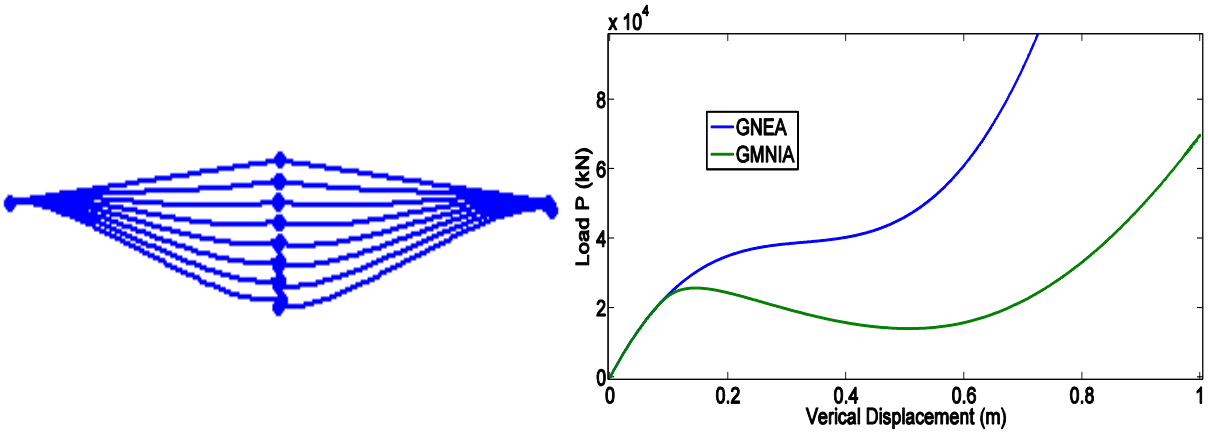

Figure 23: Deformed shape and comparison between GNEA and GMNIA

5.4 Lee's frame

The frame shown in Figure 24, was first analyzed by Lee (1968) considering linear elastic behavior. It has been also numerically studied by several authors, including Cichon (1984), Simo and Vu – Quoc (1986) and Coulter and Miller (1988). The special feature of this problem emerges from the geometrically nonlinearity point of view, as the solution reveals a very interesting equilibrium path including both snap – through and snap – back phenomena.

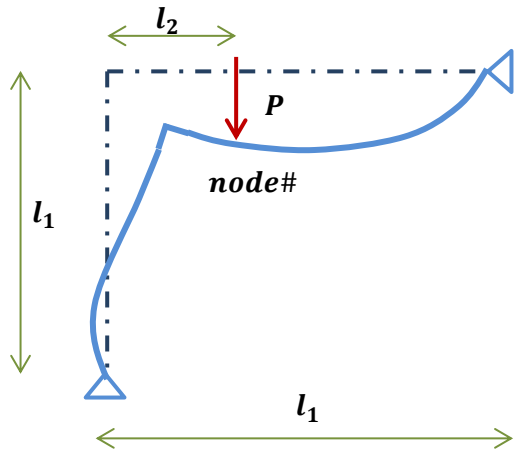

Figure 24: Lee's Frame

Table 5: Lee's Frame Properties

Length , l_1	1.20 m
Length, l_2	0.24 m
Section Height, h	20.0 mm
Section Width, b	30.0 mm
Young Modulus, E	70608.0 MPa
Yield Stress, σ_y	1020.0 MPa

In Figure 25 the differences among the different analyses are shown for the case of elastic material behavior. Notice that use of the OpenSees's force based element requires a fine discretization in order to capture the response accurately. Furthermore the same requirement also applies for the SeismoStruct analysis.

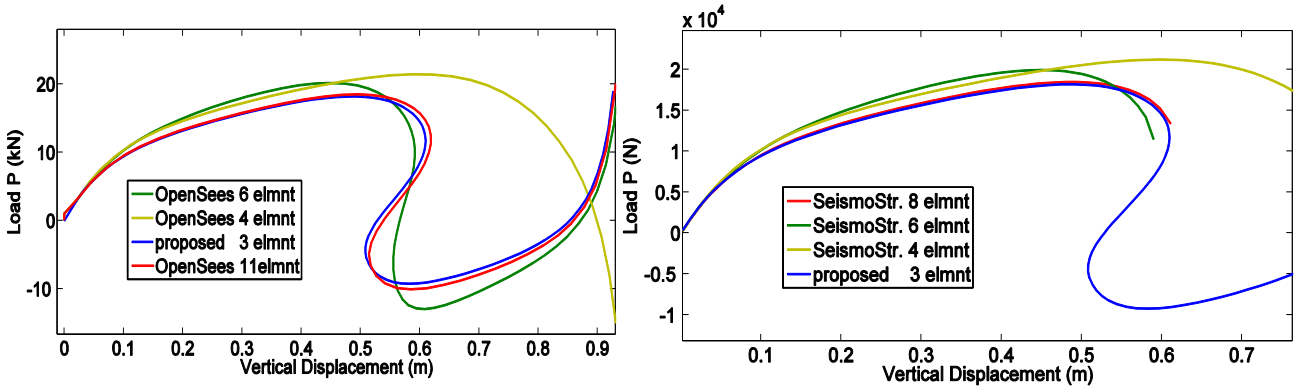

Figure 25: Equilibrium paths for different elastic analyses (node #)

The proposed element seems to peform accurately with a coarse discretization of one element per member. SeismoStruct analysis stops not because of ineffectiveness of the utilized element but due to lack of an arc – length integrator, thus the analysis was performed with a displacement control approach.

Figure 26 depicts the results of the elastoplastic analyses of Lee's frame. As for the elastic case more elements are needed to established accurate results using both Opensees and Seismostruct as compared to the proposed element.

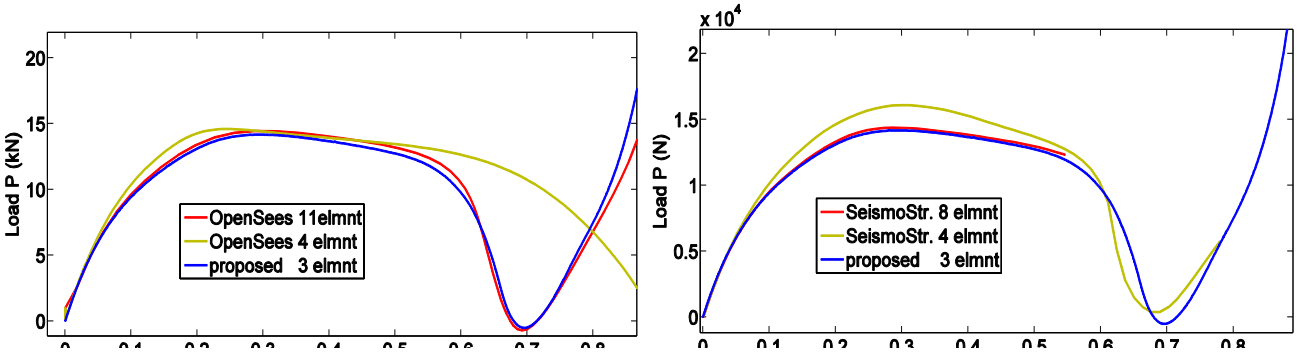

Figure 26: Equilibrium paths for different inelastic analyses (node #)

As far as the special features of the elastoplastic analysis are concerned, we see that snap – back is not manifested because of the evolution of plastic deformations. However snap – through persists becoming more intense but less steep. In general we can conclude that the presence of plasticity smoothens the distance among the peaks of the elastic solution, obtaining an intermediate path. In Figure 27 the deformed shape viewer as obtained by

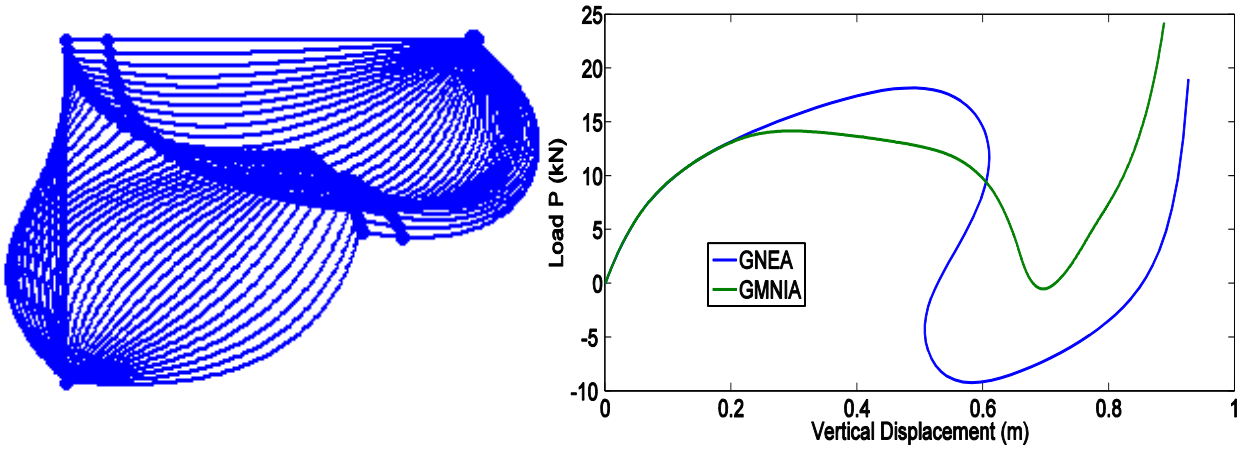

Figure 27: Deformed shape and comparison between GNEA and GMNIA

NAFS's result interface along with the final elastic and elastoplastic results are depicted.

6 Concluding Remarks and Future Research

6.1 Concluding Remarks

In this work a beam – column element is developed suitable for geometrical and material nonlinear analysis of frame structures based on primal – dual nonlinear optimization methods and variational principles. The minimization problem concerning the Total Potential Energy functional, is augmented by introducing Lagrange multipliers which handle compatibility requirements. This procedure is used to derive a hybrid three – field finite element. The internal field of rotation θ along the element was approximated via a curvature based interpolation. The other fields involved in the final formulation (forces and nodal displacements) are surface fields, thus constant in case of beam elements.

In order to derive the stress resultants in every position of the element and account for plasticity at the cross sections the concept of fiber discretization was adopted introducing the notion of distributed plasticity along the element. Fibers were assumed to exhibit a bilinear elastoplastic behavior under the additional Euler – Bernoulli assumptions, thus defining the source of elastoplastic behavior of the element.

In addition, the formulation presented incorporates large displacement theory, without introducing any simplifications for the generalized strains (curvature and axial deformation). For the compatibility constraints the integral expressions of the element displacements where utilized. That enriched the numerical formulation with the necessary geometrically nonlinear information and allowed for the exact equations to be implemented. It turns out that the proposed formulation treats displacements as integrals of deformations and not deformations as derivatives of displacement fields.

Moreover, the solution method was established via both standard Newton – Raphson and arc – length numerical schemes in order to meet the demands of every structure's equilibrium

paths. The proposed element was finally validated in comparison with the force based elements of OpenSees and SeismoStruct codes. The three elements were utilized in four well – known nonlinear benchmark problems of the literature and numerical results revealed that the proposed element allows for coarser discretization of the structural members, tracing accurately the actual equilibrium paths.

6.2 Future Research

There are various interesting topics and aspects that were not investigated herein. Therefore, some directions for further improvement of the present work are listed below:

- Extension of the formulation to include shear deformations. The element in present form does not include shear effects. However there is a significant category of structures and problems were the assumption that plane sections remain plane and perpendicular to the curved axis (Euler – Bernoulli assumption), thus ignoring shear deformations, leads to significant diferences from actual response.
- Derivation of a 3D beam – column element with the same features. The proposed element was formulated only for planar problems.
- Extension of formulation to curved beams. This extension aims at deriving quick solutions for curved beams mainly used in bridges. Furthermore such extensions may lead to interesting approximations relevant to shell problems.
- Implementation of the proposed element in dynamic nonlinear structural analysis, via a consistent mass matrix.
- Investigation of the problem's solutions without Newton's Method but utilizing sequential quadratic programming techniques to avoid inversion of the hessian matrix.

References

Meek, J. L., and Tan, H. S. (1984). "Geometrically nonlinear analysis of space frames by an incremental iterative technique." *Comput. Methods Appl. Mechs. Engrg.*, 47, 261-262.

Luenberger, D. G. and Yinyu, Y. (2008). "Linear and Nonlinear Programming", *Springer*, 3rd Edition.

Crisfield, M. A. (1981). "A fast incremental/ iterative solution procedure that handles snap through*." Computers & Structures*, 17, 55 – 62.

Felippa, C. "Advanced finite element methods".

Washizu, K. (1975). *Variational methods in elasticity and plasticity*. Pergamon Press, 2nd Edition.

Crisfield, M. A. (1991). "Nonlinear finite element analysis of solids and structures." *John Wiley & Sons Ltd*, vol. I – II.

Zienkiewicz, O. C. and Taylor, R. L. (2000). *Finite element method*, Butterworth Heinemann, 5th Edition.

Bathe, K.-J., and Bolourchi, S. (1979). "Large displacement analysis of three dimensional beam structures." *Int. J. Numer. Meth. Engng.*, 14, 961-986.

Saje, M. (1990). "A variational principle for finite planar deformation of straight slender elastic beams." *Int. J. of Solids & Struc.*, 26, 887-900.

Chan, S. L. (1988). "Geometric and material non-linear analysis of beam-columns and frames using the minimum residual displacement method." *Int. J. Numer. Methods Engrg.*, 26, 2657-2669.

De Souza, R. M. (2000). "Force-based finite element for large displacement inelastic analsysis of frames." Ph.D. thesis, Univ. of California at Berkeley, Berkeley, CA.

Cichon, C. (1984). "Large displacements in-plane analysis of elastic-plastic frames." *Comput. Struct*, 19, 737-745.

Frish-Fay, R. (1962). *Flexible bars*, Butterworths, London.

Lee, S., Manuel, F. S., and Rossow, E. C. (1968). "Large deflections and stability of elastic frames." *J. Engrg. Mech. Div., ASCE,* EM2, 521-547.

Williams, F. W. (1964). "An Approach to the non-linear behaviour of the members of a rigid jointed plane framework with finite deflections." *Quart. Journ. Mech. and Applied Math*, 17(Pt. 4), 451-469.

Lo, C. C., and Das Gupta, S. (1978). "Bending of a nonlinear rectangular beam in large deflection." *J. Appl. Mech., ASME*, 45, 213-214.

Crisfield, M. A. (1990). "A consistent co-rotational formulation for non-linear, three dimensional beam elements." *Comput. Methods Appl. Mech. Engrg*, 81, 131-150.

Wood, R. D., and Zienkiewicz, O. C. (1977). "Geometrically nonlinear finite element analysis of beams, frames, arches, and axisymmetric shells." *Comput. Struct.*, 7, 725-735.

Coulter, B. A., and Miller, R. E. (1988). "Numerical analysis of a generalized plane 'elastica' with non-linear material behaviour." *Int. J. Numer. Methods Engrg.*, 26, 617-630.

Cichon, C. (1984). "Large displacements in-plane analysis of elastic-plastic frames." *Comput. Struct*, 19, 737-745.

Simo, J. C., and Vu-Quoc, L. (1986). "A three-dimensional finite strain rod model: Part 2: Computational aspects." *Comput. Methods Appl. Mech. Engrg.*, 58, 79-116.

Neuenhofer, A., and Filippou, F. C. (1998). "Geometrically nonlinear flexibility-based frame finite element." *J. Struct. Engrg., ASCE*, 124, 704-711.

Spillers, W. R. and MacBain K. M. (2009). *Structural optimization*. Springers, New York.